Final Progress Report:

Title Page

Grant Number: 5R21OH010490-02

FAIN: R21OH010490

Principal Investigator(s):

Matthew Wolf Foster, PHD

Scott M Palmer (contact), MD

Project Title: Proteomics of flavorings-induced airway disease

Duke Administrative contact: John M. Michnowicz

Exec Dir, Off of Research Admn

Duke University

2200 West Main St.

Suite 820 Erwin Square Plaza

Durham, NC 277050000

Award e-mailed to: gcmail@mc.duke.edu

Project Period: 09/01/2014 – 08/31/2016

Date report completed 1/16/17

Principal Investigator(s):
Matthew Wolf Foster, PHD
Scott M Palmer (contact), MD
Project Title: Proteomics of flavorings-induced airway disease

Table of Contents

Principal Investigator(s):

Matthew Wolf Foster, PHD

Scott M Palmer (contact), MD

Project Title: Proteomics of flavorings-induced airway disease

Abstract: The overall goal of our research is to improve the diagnosis and treatment of bronchiolitis obliterans (BO) that occurs in the workplace as a result of exposure to artificial flavors. Workers in the food manufacturing industry are at significant risk for occupational airway disease due to exposure to commonly used artificial flavorings. In particular, diacetyl (DA) used in butter flavoring has been linked to the development of bronchiolitis obliterans (BO), an irreversible airway fibrosis. As a result, NIOSH NORA objectives include strategic goals focused on work-related airway diseases, specifically targeting studies of "diacetyl and other potentially harmful artificial flavorings" to improve workplace risk assessment (Goal 5.2.2) and define mechanisms of toxicity (Goal 5.1.3). This proposal directly addressed the NIOSH objectives for the Manufacturing Sector and Respiratory Disease Cross-sector. Under the R21 two year funding mechanism progress was completed towards the primary goal of this project to identify novel biomarkers of early lung injury after exposure to the artificial flavors such as DA. We treated human bronchial epithelial cells (NHBE) cells with DA in occupationally relevant concentrations. We then demonstrated differential expression of proteins (i.e. the secretome) basally, apically, and intracellularly from cultured NHBE *in vitro* at an air-liquid interface in response to DA using state-of-the-art proteomic analysis technology. The study specific aims as performed were to 1) **Quantify changes in the basolateral and apical secretomes of NHBE cells grown under physiological conditions after exposure to DA and determine the cellular pathways activated by flavoring exposures and** 2) **Quantify changes in the intracellular proteome and phosphoproteome of NHBE cells grown under physiological conditions after exposure to DA and determine the cellular pathways activated by flavoring exposures.** Our unbiased discovery based approach has identified potential novel biomarkers of flavoring toxicity that could improve early recognition of airway toxicity in the workplace and will provide new insights into disease mechanisms if validated through further in vitro and in vivo studies.

Section 1 of the Final Progress Report:

Significant or Key Findings: The overall goal of our research is to improve the diagnosis and treatment of bronchiolitis obliterans (BO) that occurs in the workplace as a result of exposure to artificial flavors. Workers in the food manufacturing industry are at significant risk for occupational airway disease due to exposure to commonly used artificial flavorings. In particular, diacetyl (DA) used in butter flavoring has been linked to the development of bronchiolitis obliterans (BO), an irreversible airway fibrosis. As a result, NIOSH NORA objectives include strategic goals focused on work-related airway diseases, specifically targeting studies of "diacetyl and other potentially harmful artificial flavorings" to improve workplace risk assessment (Goal 5.2.2) and define mechanisms of toxicity (Goal 5.1.3). This proposal directly addressed the NIOSH objectives for the Manufacturing Sector and Respiratory Disease Cross-sector.

The R21 study has a **primary goal** to identify novel biomarkers of early lung injury after exposure to the artificial flavors such as DA. We treated human bronchial epithelial cells (NHBE) cells with DA in occupationally relevant concentrations. We then demonstrated differential expression of proteins (i.e. the secretome) basally, apically, and intracellularly from cultured NHBE *in vitro* at an air-liquid interface in response to DA using state-of-the-art proteomic analysis technology. Our unbiased discovery based approach has identified potential novel biomarkers of flavoring toxicity that could improve early recognition of airway toxicity in the workplace and will provide new insights into disease mechanisms if validated through further in vitro and in vivo studies.

Proteins involved in matrix organization, degradation and turnover were abundantly present in both the apical and basolateral secretomes. As an example, we identified PGBM (perlecan) to be robustly increased in the apical secretome. Proteins that are known to degrade ECM and facilitate matrix turnover including MMP9, TIMP1 and TIMP2 were increased. DDR1 is another novel protein identified in our data set. DDR1 is a cell surface receptor for fibrillar collagen with tyrosine kinase activity that regulates cell attachment to and remodeling of the ECM, cell migration, differentiation, survival and cell proliferation. These observations taken together lend weight to the notion that soluble factors derived from the airway epithelium could be driving BO lesion development by fundamentally altering the matrix in the subepithelial space. MMP-9 and TIMP1 were elevated in both the apical and basolateral secretomes after DA exposure and have previously been observed to be increased in BO, particularly in the clinical context of lung transplant and in pre-clinical experimental models. These observations that independently replicate our results in other pre-clinical and clinical studies of BO further support that the airway epithelium may actively participate in directing matrix remodeling after DA exposure.

In studies at an intercellular protein level identified quantified approximately 3,400 proteins and 5,700 phosphopeptides from the well-differentiated human primary tracheobronchial epithelial cell cultures after repeated exposures to occupationally-relevant doses of diacetyl vapor. Diacetyl-exposed cells showed a marked reduction in proteins and phosphopeptides related to cilia structure-function, and extensive injury to ciliated cells was confirmed by staining of airway culture sections. Conversely, a protein signature of squamous metaplasia was markedly elevated following diacetyl exposure. This signature correlated with apparent transglutaminase-mediated crosslinking of basal cell cytokeratins and the suprabasal expression of repetin, a marker of terminal squamous differentiation. Diacetyl vapor exposure also led to large increases in phosphorylation of previously uncharacterized sites in the head and tail domains of cytokeratins K6 and K14. Collective, these results suggest that basal cell differentiation, and squamous metaplasia, may represent a precursor to flavoring-induced BO.

In summary we have observed polarized and highly regulated changes in intracellular and secreted protein expression in response to DA vapor exposure in human airway epithelial cells. In response to DA, the secretome is enriched for proteins associated with matrix remodeling and

intracellular changes suggest activation of basal cells in response to epithelial squamous metaplasia. Translation of findings: These results taken as a whole support the notion that the epithelium may actively direct the fibroproliferative response of the underlying mesenchyme and may serve as a regulator of BO pathobiology. The present results further suggest several potential proteins and/or pathways that could be targeted in future studies to further understand disease pathobiology or to intervene in early disease development. Finally, consistent with our overall aims, our work provides several novel protein targets that could be pursued as potential biomarkers of DA exposure that could be useful in identifying workers at higher risk for BO. As an exploratory R21 grant with limited scope and funding, we have achieved the goal of identifying potential targets for further validation and study in human samples from exposed workers.

Research Impact: Impact in the workplace will depend upon further validation and testing of candidate protein biomarkers but provides ample candidates for hypothesis testing in further in vivo and human studies.

Scientific Report.

In support of the overall research goal, the study objectives efforts during the two year R21 focused entirely on the proteomic analysis of the in vitro model. The original second aim was modified to reflect further in depth characterization of the protein effects at an intracellular level and phosphoprotein level given the unique capability that became available to pursues these additional studies at Duke in parallel with the secreted protein analysis. In vivo targeted validation studies were not completed due to the effort required to complete the first two aims below but remain a goal in future studies. The work below provides the most complete picture of the cellular effects of DA exposure upon the airway epithelium ever reported. Studies were divided into analysis of the secreted proteins and intracellular protein and phosphoprotein changes and detailed report for each is provided below:

Specific Aims (as completed):

Aim 1. Quantify changes in the basolateral and apical secretomes of NHBE cells grown under physiological conditions after exposure to DA and determine the cellular pathways activated by flavoring exposures.

Background:

Bronchiolitis obliterans (BO) is an increasingly important human disease now recognized in a variety of clinical contexts including autoimmune diseases, as a consequence of lung or bone marrow transplantation, or as a result of occupational exposures. Histologically, BO is characterized by airway centered fibrosis that can cause partial or total airway occlusion. Clinically, BO results in significant decrements in lung function, and can progress to disability or death. Diacetyl (DA; 2-3-butanedione) is a volatile □-diketone that occurs naturally as a result of fermentation and that has most commonly been used to impart a buttery aroma and flavor to microwave popcorn, flavored coffee and e-cigarettes. Growing evidence now shows that occupational exposure to DA vapor is associated with the development of BO in the microwave popcorn industry, in the food flavoring manufacturing industry {Kim, 2010 #924} and in the manufacture of diacetyl itself. Despite increasing recognition of occupational BO, the mechanisms that lead to its development remain poorly understood. BO-inducing toxins such as DA are first encountered by the airway epithelium. As such, the early secretory response of the airway epithelium after DA exposure may be central in the pathogenesis of BO.

To better understand the epithelial response to DA and the role it may play in the lesion development that is characteristic of BO, we have taken an unbiased proteomic approach using primary human epithelial cells from multiple independent donors. We report changes in protein secretion in the apical and basolateral compartments and changes intracellularly in protein and phosphoprotein expression of fully differentiated primary human airway epithelial cells after repeated exposure to DA vapor, providing new insights into early events that may contribute to flavoring induced airways disease.

MATERIALS AND METHODS

Cell Culture

Air-liquid interface cultures of passage two tracheobronchial epithelial “EpiAirway AIR-100” cells, from 4 normal donors, were purchased from MatTek (Ashland, MA). The cells were maintained at 37 °C in a 5% CO_2 atmosphere for the duration of the experiments. The apical and basolateral compartments were maintained and treated as follows:

The apical surface of each transwell was washed gently 3x with 200 □L of PBS prior to the beginning of the experiment and daily thereafter; all washes were retained and stored at -80 °C for later analysis. On Day 0 (D0), D2 and D4, after the washing of the apical surface, 50 ul of 25 mM DA was placed in the porous insert of a cap that was then sealed over the cells with silicone. We have previously determined that this system generates a clinically relevant vapor exposure of approximately 1000 ppm {Kelly, 2014 #961}. PBS was used as a control, and the cells were exposed for one hour on every exposure day. On D6, the apical surface of the cells was washed a final time, and the samples were stored at -80 °C for proteomic analysis.

The media in which the basolateral compartment was immersed was changed daily and retained at -80 °C for later analysis.

Proteomic Analysis

Measures of analytical versus biological variability. In order to assess technical reproducibility, we calculated the % coefficient of variation (%CV) for each protein across the triplicate injections of a QC pool at the beginning, middle and end of the basolateral and apical analyses. For the apical samples, the mean %CV of the QC pools was 24.5% for all proteins and 15.4% for proteins quantified by 2 or more peptides. For the basolateral secretome, the average %CVs for the QC pools was 17.3% for all proteins and 11.5% for proteins quantified by 2 or more peptides. The quantitative reproducibility of replicate QC injections was also reflected in the principal component analyses for proteins quantified by 2 or more peptides. As expected, the QC pools were very tightly clustered and were centered between the PBS- and DA-exposed groups. In both the apical (Figure S1) and basolateral secretomes (Figure S2), the DA-exposed cells from donor 9831 were isolated from the others along PC2.

Quantitative analysis of protein expression in the secretomes of PBS- and DA-exposed cells. The data were imported into Rosetta Elucidator followed by mass and retention time alignment, database searching of MS/MS spectra and quantitation of area-under-the-curve of identified features. Following database searching and peptide scoring using PeptideProphet, the apical data were annotated at a 0.9% peptide false discovery rate, resulting in identification of 4,273 peptides and 1,046 proteins, and the basolateral data were annotated at a 1% peptide FDR, resulting in identification of 6067 peptides and 1327 proteins. After filtering the data to remove low quality peptides with poor chromatographic peak shape, and scaling of the data to the robust median across all samples, a total of 3,077 peptides (Table S1) and 1,046 proteins (Table S2) were quantified across all apical samples, and 6,067 peptides (Table S3) and 1327 proteins (Table S4) were quantified across all basolateral samples.

RT-PCR. Total cellular RNA was isolated using RNAqueous4PCR isolation kit (Invitrogen), and converted to cDNA for analysis (Invitrogen). mRNA levels were evaluated by Taqman using the following probe sets (Thermo Fisher Scientific; Waltham MA): - PTPRS (Hs00370080_m1); FBLN3 (Hs00244575_m1); DDB1 (Hs01096550_m1); ECM1 (Hs00189435_m1); and GDF15 (Hs00171132_m1), using Beta Actin (4326315E) as an endogenous control. Ct values were determined using ABI 7500 RealTime PCR System (Thermo Fisher Scientific). Changes in expression were calculated using the 2- Ct method.

Statistical Analyses. Peptide- and protein-level expression values were log-2 transformed and features with missing or low abundance measurements in greater than half of the samples were not subject to further statistical analysis. Remaining low abundance measurements were set to

the 5th percentile of the empirical distribution of overall intensities. Proteins having greater than 30% technical variability, those quantified with a single peptide, and non-human experimental control proteins were not subject to further analyses. The total number of proteins meeting these criteria was 541 in the apical secretome, and 793 in the basolateral secretome. The first three principal components of the normalized protein expression values were then computed for both the apical and basolateral compartments, and visualized with respect to donor and treatment. Statistical assessment of differential expression between PBS and DA exposure was carried out using a paired t-test by donor in each secretome compartment. The resulting p-values were corrected for multiple testing by controlling the false discovery rate of 0.10 with the Benjamini-Hochberg method.

Unsupervised agglomerative clustering of the resulting significantly differentially expressed apical and basolateral protein sets were performed using the Euclidean distance metric and Ward linkage method. Differentially expressed protein sets were subdivided into those up-regulated (positive fold change), or down-regulated (negative fold change) with DA exposure, and quantitative pathway enrichment analysis of the protein sets were carried out with the REACTOME pathway analysis tool. Protein-protein interactions within our data sets were visualized using the publicly available STRING suite of analysis tools.

RESULTS

1. *Proteomic analysis of DA-exposed primary human airway epithelial cells in ALI culture reveals that variability in protein expression is driven by the exposure.* Our proteomic analysis identified 541 apical and 793 basolateral proteins by more than 2 individual peptides and with less than 30% technical variability as described in Materials and Methods. Unsupervised hierarchical clustering analysis of these proteins resulted in the apical secretome segregating by exposure (Figure 1). The basolateral secretome also segregates by exposure, with the exception of donor 9831 (Figure 2). These results show that DA exposure largely underlies the variability in the protein expression data. Similarly, in a principal components analysis, both the apical (Figure S1) and basolateral (Figure S2) secretomes segregated by exposure. While the proteomic response of donor 9831 varied somewhat from the responses of the other donors showing the presence of inter-individual variation in the response to DA, the principal component analysis supports that the greatest variability in the data was due to DA exposure.
2. *Proteomic analysis of DA-exposed primary human airway epithelial cells in ALI culture reveals a highly polarized secretory response.* Using a paired t-test to evaluate changes in protein expression across all 4 donors and an FDR-adjusted p-value of less than 0.1 as described in Materials and Methods, we show in Figure 3 that after DA exposure there were 61 significantly differentially expressed proteins unique to the apical secretome (Table 1) and 81 significantly differentially expressed proteins unique to the basolateral secretome (Table 2). We identified an additional 11 proteins that were present in both the apical and basolateral secretomes 72 (Table 3).
3. *DA exposure of primary human airway epithelial cells in ALI culture induces a matrix remodeling proteomic signature*. To determine whether broad categories of proteins were over-represented in our data set, we performed pathway enrichment analysis on the proteins identified in Tables 1 and 2 using the publicly available REACTOME database. In the apical secretome, we observed that proteins with increased expression were over-represented in pathways that are important in extracellular matrix degradation, matrix organization and cell-cell interactions (Table 4). These include laminins (LAMC2, LAMA3 and LAMB3), perlecan (PGBM), E-cadherin (CADH1), as well as MMP9, MMP10 and TIMP1. Conversely, we observed that proteins with decreased expression in the apical secretome were over-represented in pathways that are important in complement activation (including complement

factor B (CFAB), CD59 and complement component 4A (CO4A)) and lipid metabolism (including phospholipid transfer protein (PLTP) and bile salt-activated lipase (CEL); Table 5). In the basolateral secretome, proteins with increased expression were over-represented in pathways important in ECM degradation and organization (including the cathepsins B and D (CATB and CATD) as well as TIMP1, TIMP2, MMP9 and MMP14) and platelet function (including adenylyl cyclase-associated protein 1 (CAP1), transferrin (TRFE), amyloid beta A4 (A4) and TIMP1; Table 6). Finally, in the basolateral secretome, proteins with decreased expression were over-represented in pathways important in ECM synthesis and assembly (including the fibrillar collagens CO1A1, CO5A2 and CO7A1, and EGF-containing fibulin-like extracellular matrix protein 1 (FBLN3); Table 7).

4. *DA exposure of primary human airway epithelial cells in ALI culture results in dysregulation of extracellular matrix organization and EGFR activation and signaling.* To further identify relationships between the differentially expressed proteins in our data set we used the STRING suite of online analysis tools to identify known protein-protein interactions {Snel, 2000 #1179}. There are several nodal interactions revealed in the apical secretome including that between MMP9, MMP10, TIMP1 and tenascin C (TENA); between proteasome subunit alpha types-3 and -7 (PSMA3 and PSMA7) and puromycin-sensitive aminopeptidase (NPEPPS); and between the Laminins A3, B3 and C2; between the histone proteins H2B1, H2AY and histone cluster4 (Figure S3).
5. In the basolateral secretome, we observed a nodal interaction centered on the EGFR and proteins that have been shown to or hypothesized to regulate the EGFR including FBLN3 (EGF-containing fibulin-like extracellular matrix protein 1, AKA EFEMP1 with EGF-like domains), DDB1 (DNA damage-binding protein 1 that contributes to EGFR signaling attenuation in C. elegans), GDF15 (growth differentiation factor 15, a member of the TGF-□ superfamily of proteins that has been shown to potentiate EGFR signaling) and ECM1 (extracellular matrix protein 1 a member of the IL-1 family of proteins that associates with perlecan in the basement membrane and can potentiate EGFR signaling) were significantly differentially expressed (Figure S4).
6. Finally, we measured individual intracellular transcript levels by RT-PCR to validate the observed changes in EGFR related proteins after DA exposure. We show in Figure 4 that DA exposure induced significant decreases in mRNA for FBLN3 and DDB1 (Figures 4A, 4B and 4C), which are known or hypothesized negative regulators of EGFR signaling. Similarly, mRNA for ECM1 and GDF15 (Figures 4D and 4E), which have been shown to potentiate EGFR signaling is increased. Parallel changes in the proteins were observed in the basolateral compartment (FBLN3 decreased -3.4 fold, DDB1 decreased -1.9 fold, ECM1 increased 9.9 fold, and GDF15 increased 3.2 fold). These observations including changes in basolateral protein expression and at an intercellular transcript level provide independent validation that DA exposure of primary human airway epithelial cells in ALI culture results in dysregulated EGFR signaling.

DISCUSSION

Clinical and experimental evidence link the development of BO to DA exposure. However, little is known about the underlying biological mechanisms that lead to disease development. In the current report we have focused on airway epithelial cells because they are the first cell type to be encountered by inhaled toxins such as DA. To begin to understand the processes that might occur after DA exposure, we have exposed fully differentiated primary airway epithelial cells from four unique donors to DA vapor concentrations or PBS as a control to model repeated occupational exposures. We then used discovery based proteomics to understand DA-induced epithelial cell responses after exposure in the apical and basolateral compartments. This study shows for the first time that the apical and basolateral secretomes of DA exposed airway epithelial cells in ALI culture are highly polarized and distinct with minimal overlap. Furthermore, we demonstrate that

the epithelial secretory response to DA in 4 independent donors is remarkably consistent, particularly in the apical secretome. Finally, we have identified novel proteins in both the apical and basal secretomes that provide new insights into mechanisms that may drive the development of BO.

In the present analysis, we have identified many proteins that have not been previously associated with BO but that could play a biologically plausible role in disease pathogenesis. For example, CXCL16 showed increased expression in the basolateral secretome. Elevated CXCL16 has previously been associated with epithelial derived lung cancers and has been shown to modulate MMP and TIMP expression including MMP9 and TIMP2, both of which show altered expression in our data set. Similarly, IL-36 showed increased expression in the basolateral secretome (Table 2). IL-36 is a member of the IL-1 superfamily of cytokines and has been shown to promote inflammation or fibrosis in chronic fibrotic skin and bowel disease but not previously in lung disease. However, exogenous IL-36 instillation in the rodent lung has been associated with neutrophil recruitment, a common feature of BO in pre-clinical rodent models and in human BO.

A particularly novel aspect of the present study is that proteins known or thought to negatively regulate EGFR signaling, including FBLN3 and DDB1 were decreased, while those known or thought to increase EGFR signaling including ECM1 and GDF15 were increased. These results were validated by parallel changes in intracellular transcripts. Taken together, the observation that both negative and positive regulators of EGFR signaling are dysregulated strongly support that EGFR signaling plays an important role in the epithelial response to DA exposure.

Another novel observation in the current data set was revealed by the REACTOME analyses that showed that proteins involved in matrix organization, degradation and turnover were abundantly present in both the apical and basolateral secretomes. As an example, we identified PGBM (perlecan) to be robustly increased in the apical secretome. Perlecan is a basement membrane protein that has been hypothesized to be fundamental to organ and tissue integrity and has been shown to have increased expression in BO after lung transplantation. Similar to our observation that perlecan is differentially expressed in the apical secretome, three other components of the basement membrane, LAMA3, LAMB3 and LAMC2 were differentially expressed in the apical secretome (Table 1). Interestingly, the fibrillar collagens that make up the basement membrane including CO5A2, CO7A1 and CO1A1 showed decreased expression in the basolateral secretome (Table 7) while proteins that are known to degrade ECM and facilitate matrix turnover including MMP9, TIMP1 and TIMP2 were increased. DDR1 is another novel protein identified in our data set. DDR1 is a cell surface receptor for fibrillar collagen with tyrosine kinase activity that regulates cell attachment to and remodeling of the ECM, cell migration, differentiation, survival and cell proliferation. These observations taken together lend weight to the notion that soluble factors derived from the airway epithelium could be driving BO lesion development by fundamentally altering the matrix in the subepithelial space.

While the current data set reveal the novel observation that the airway epithelium could be playing an active role in driving remodeling of the matrix in developing BO lesions, a number of matrix remodeling proteins identified in the current analysis have already been implicated as associated with BO, thus providing additional validation for the biological relevance of our results. As examples, MMP-9 and TIMP1 were elevated in both the apical and basolateral secretomes after DA exposure and have previously been observed to be increased in BO, particularly in the clinical context of lung transplant and in pre-clinical experimental models. Similarly, we have previously shown experimentally in our rodent model of occupational BO that TENA (tenascin C), upregulated apically in our current study, had increased protein expression in the subepithelial space of developing BO lesions. These observations that independently replicate our results in other pre-clinical and clinical studies of BO further support that the airway epithelium may actively participate in directing matrix remodeling after DA exposure.

Similar to other in vitro investigations, this study has clear strengths and limitations. A unique strength of the current study is that we used brief repeated exposures to DA vapor to replicate exposure to occupationally relevant concentrations of inhaled DA. Another strength of the present study is that we examined the response of airway epithelial cells from four independent human donors. Because human subjects are genetically diverse, this approach had the potential to yield highly variable results. However, we observed that the response of the individual donors was strikingly consistent, making our results much more generalizable than many previous studies that have relied upon cells from a single human donor. Despite these strengths we recognize our work also has several limitations: First, while primary airway epithelial cells are grown at air liquid interface accurately reproduce their in vivo environment, the basement membrane they synthesize is likely incomplete when compared with the basement membrane on which they reside in vivo. Similarly, the mesenchymal cells that would normally lie beneath this basement membrane are absent. In vitro studies on ALI epithelial cultures in which a basement membrane and the underlying mesenchyme are present are now possible and will be pursued in the future. Second, we did not perform direct validation of specific differentially expressed proteins; however, we did directly validate intracellular transcript changes that correlated with changes in EGFR regulated proteins. In addition, several proteins we identified as elevated (MMP9 and TIMP1) have also been reported elevated in preclinical or clinical models of BOS providing an additional confidence in the current results. Finally, we recognize the limitations of resolution inherent to proteomic technology and we acknowledge that low-abundance proteins may be below the limits of detection of the technology.

Conclusions:

In summary we have observed polarized and highly regulated changes in protein expression in response to DA vapor exposure in human airway epithelial cells. Importantly the significant changes in protein expression observed in the apical and basolateral secretomes were reproduced in all four independent human donors. In response to DA, the secretome is enriched for proteins associated with matrix remodeling and that regulate signaling through the EGFR. These results taken as a whole support the notion that the epithelium may actively direct the fibroproliferative response of the underlying mesenchyme and may serve as a regulator of BO pathobiology. The present results further suggest several potential proteins and/or pathways that could be targeted in future studies to further understand disease pathobiology or to intervene in early disease development. In addition, our work provides several novel protein targets that could be pursued as potential biomarkers of DA exposure that could be useful in identifying workers at higher risk for BO.

Specific Aim 2. Quantify changes in the intracellular proteome and phosphoproteome of NHBE cells grown under physiological conditions after exposure to DA and determine the cellular pathways activated by flavoring exposures.

INTRODUCTION

The inhalational exposure of workers in the microwave popcorn, baked goods and coffee manufacturing industries to the “artificial butter” flavor 2,3-butanedione (diacetyl, DA) has been linked to the development of bronchiolitis obliterans (BO), a condition of fixed obstructive lung disease and small airway fibrosis. These cases have led to strict limits on workplace DA exposure, but questions remain as to the potential toxicities of DA substitutes, including the related α-diketone 2,3,-pentanedione (PD), and of the possibility of as yet unidentified exposures to DA and PD. In addition, there is increasing awareness of the use of DA and PD in e-cigarette flavors,

raising the possibility that use of e-cigarettes may increase risk for airways disease through a similar mechanism.

Rodent models have been critical to the demonstration that respiratory exposure to DA and PD can lead to the development of BO, and suggest this process begins with epithelial injury. We have shown in rats, that intratracheal instillation of DA leads to a rapid loss of acetylated tubulin (a cilia marker), followed by sloughing of the epithelium and finally airway fibrosis at these sites of severe injury. This is consistent with the idea that denudation of the epithelium may be necessary for the development of toxicant-induced BO. However, epithelial ablation alone is unlikely to explain the entire spectrum of flavoring-induced airway disease, as the airways of exposed rodents also show evidence of squamous metaplasia and keratinization.

To better understand the injury process, we have begun to study the effects of diacetyl vapor on the human airway epithelium. Specifically, we have utilized air-liquid interface cultures of differentiated human tracheobronchial epithelial cells (TBECs) to model effects of repeat 1 h exposures to ~1000 ppm vapor, conditions that mimic a high occupational exposure. In this model, we previously reported shedding of the pro-inflammatory and pro-fibrotic EGFR ligand amphiregulin by TBECs after repeated exposures to DA. While these data suggest a potential mechanism for flavoring-induced fibrosis, they do not reveal the full extent of the pathological effects of DA on the airway epithelium. Recently, Fedan and coworkers also found that a 6 h exposure of differentiated normal human bronchial epithelial cells to as little as 100 ppm DA caused cell death based on histological assessment. Here, we have sought to utilize a more comprehensive 'omic approach to flavoring-induced epithelial injury, beginning with an analysis of the whole cell proteome and phosphoproteome of differentiated TBECs after repeated exposures to DA vapor.

METHODS

In vitro model of diacetyl exposure. Exposures of tracheobronchial epithelial cells (TBECs) to DA vapor were as previously-described {Kelly, 2014 #8}. Briefly, passage two TBECs (MatTek EpiAirway™) were from 4 individual healthy male, nonsmoker human donors (with no disease or medication history at time of tissue procurement). Additional characteristics were: Donor 1 (Cat# 9831, Caucasian, age 23); Donor 2: (Cat# 11257, Caucasian, age 23); Donor 3: (Cat# TBE-20, Caucasian, age 13); Donor 4 (Cat# TBE-30, Hispanic, age 50). Cells were cultured on transwells (9 mm internal diameter) and fully-differentiated at air-liquid interface. Cells were exposed to a vapor cup containing 50 µl of 25 mM DA in PBS (or PBS vehicle control), for 1 h on days 0, 2 and 4 and were harvested on day 6. Apical surfaces were washed with PBS prior to each exposure, and basolateral media (MatTek AIR-100) was exchanged each day. Cells which were harvested for proteomics were cultured in protein-free basolateral media (DMEM:F12 w/ high glucose and w/o pyruvate),1.5 mM Hepes, 0.3 mM $MgCl_2$, 1 mM $CaCl_2$, 80 µM ethanolamine, 0.5 mM $MgSO_4$, 100 nM all-trans-retinoic acid) between days 5 and 6, and apical surfaces were rinsed with PBS prior to freezing. Cells harvested for immunofluorescence were cultured in AIR-100 media for the entirety of the experiment and after PBS wash, were formalin-fixed and paraffin embedded.

Sample preparation for proteomics. Three wells of TBECs per donor per condition were lysed by scraping with 50 mM ammonium bicarbonate pH 8.0 (AmBic) containing 0.2% acid labile surfactant (ALS-1), 5 mM NaF, 1 mM Na_3VO_4 and 10 nM calyculin, followed by probe sonication (3 x 3 s). After centrifugation, protein recovery was quantified by Bradford assay, and 250 µg of protein per sample was denatured and reduced by addition of 10 mM DTT followed by heating at 80 ºC for 10 min. Next, alkylation was performed by addition of 25 mM iodoacetamide and incubation in the dark for 30 min. TPCK-trypsin (1:50 w/w trypsin:protein) was added, and proteins were digested at 37 ºC overnight. Samples were then acidified with 1% trifluoroacetic acid (TFA)

and 2% acetonitrile (MeCN), followed by heating at 60 ºC for 2 h, to inactivate trypsin and to degrade ALS-1. Approximately 25 µg of peptide was removed for proteome analysis, spiked with 50 fmol/µg of trypsinized yeast alcohol dehydrogenase 1 (MassPrep; Waters) and frozen at -80 ºC.

Phosphopeptide enrichment. Trypsinized bovine casein was added to the remaining 225 µgs of peptide digests at 30 fmol/µg and the peptides were lyophilized to dryness. Dried peptides were reconstituted in 80% MeCN containing 1% TFA (binding buffer) and enriched using 200 µg capacity tips (GL Sciences) using the manufacturer recommended protocol. After binding, two washes were performed with binding buffer containing 1M glycolic acid to reduce binding of non-phosphorylated peptides. After high pH elution and neutralization, peptides were lyophilized and subjected to C18 Stage tip purification. Finally, after an additional lyophilization, peptides were resuspended in 20 µl of 10 mM citrate, 2% MeCN, 1% TFA containing 10 fmol/µl of trypsinized yeast ADH1 and were transferred to Maximum Recovery LC vials (Waters). QC pools were prepared by pooling 5 µl of all samples.

Quantitative mass spectrometry analysis of the TBEC proteome. Quantitative one-dimensional liquid chromatography, tandem mass spectrometry (1D-LC-MS/MS) was performed on 250 ng of the peptide digests per sample in singlicate, with additional QC and conditioning analyses as described in Table S1. Samples were analyzed using a nanoACQUITY UPLC system (Waters) coupled to a QExactive Plus high resolution accurate mass tandem mass spectrometer (Thermo) via a nanoelectrospray ionization source. Briefly the sample was first trapped on a Symmetry C18 300 mm × 180 mm trapping column (5 µl/min at 99.9:0.1 v/v H_2O:MeCN) followed by an analytical separation using a 1.7 um ACQUITY HSS T3 C18 75 mm × 250 mm column (Waters) with a 90 min gradient of 5 to 40% MeCN with 0.1% formic acid (buffer B) at a flow rate of 400 nl/min and column temperature of 55 °C. Data collection on the QExactive Plus MS was performed in data-dependent acquisition (DDA) mode with a 70,000 resolution (@ m/z 200) full MS scan from m/z 375 to 1600 with a target AGC value of 1e6 ions followed by 10 MS/MS scans at 17,500 resolution (@ m/z 200) at a target AGC value of 5e4 ions. A 20 s dynamic exclusion was employed. The raw data for this experiment was deposited at Chorus Project (www.chorusproject.org) under the project “EpiAir Diacetyl Proteomics” and experiment “EpiAir Diacetyl Proteome”.

Quantitative mass spectrometry analysis of the TBEC phosphoproteome. Quantitative one-dimensional liquid chromatography, tandem mass spectrometry (1D-LC-MS/MS) was performed on 4 µl (20%) of the enriched peptide digests per sample in singlicate, with additional QC and conditioning analyses as described in Table S4. Samples were analyzed using a nanoACQUITY UPLC system (Waters) coupled to a QExactive Plus as above except that the analytical separation used a 5 min hold at 3% MeCN/0.1% FA followed by a 90 min gradient of 3 to 30% buffer B. The raw data for this experiment was deposited at Chorus Project (www.chorusproject.org) under the project “EpiAir Diacetyl Proteomics” and experiment “EpiAir Diacetyl Phosphoproteome”.

Label-free quantitation. For quantitation of each dataset, eleven raw data files (including QC analyses) were imported into Rosetta Elucidator v3.3 (Rosetta Biosoftware, Inc), and LC-MS runs were aligned based on the accurate mass and retention time of detected ions (“features”) using the PeakTeller algorithm in Elucidator. Relative peptide abundance was calculated based on area-under-the-curve (AUC) of aligned features across all runs. The proteome had 268,024 quantified features, and the phosphoproteome had 214,345 quantified features.

MS/MS data was processed using Mascot Distiller (Matrix Science), which produced 463,245 and 416,476 high collision energy (peptide fragment) spectra for the proteome and phosphophoproteome datasets, respectively. Database searches were Mascot Server (version

2.5, Matrix Sciences) against a custom Swissprot database with *Homo sapiens* taxonomy (downloaded on 02/12/14) with additional proteins, including yeast ADH1 and bovine casein, as well as an equal number of reversed-sequence "decoys" for false discovery rate determination (40,546 total entries). Mascot Distiller and Mascot Server were utilized to produce 463,245 that were subjected to database searching. Search parameters for the proteome analysis included fixed modification on Cys (carbamidomethyl) and variable modifications on Met (oxidation), Asn/Gln (deamidation). Search parameters for the phosphoproteome analysis included fixed modification on Cys (carbamidomethyl) and variable modifications on Met (oxidation), Ser/Thr (phosphorylation) and Tyr (phosphorylation). The proteome data was annotated at a 0.5% false discovery rate (FDR) after individual peptide scoring using the PeptideProphet algorithm in Elucidator. The phosphoproteome data was annotated at a ~0.5% peptide FDR using a Mascot Ion Score of 20. Finally, the phosphoproteome data was analyzed within Rosetta Elucidator using ModLoc, a probability-based phosphorylation site localization tool based on the AScore algorithm {Beausoleil, 2006 #6}. For quantitative processing, the data was first curated to contain only high quality peptides with appropriate chromatographic peak shape and the dataset was intensity scaled to the robust median across all analyzed samples.

Statistical Analysis. Statistical tests were performed in Rosetta Elucidator unless otherwise noted. Briefly, an intensity floor value of 1 was given to missing data followed by a log2 transformation. A two-sample paired t-test was performed, with or without Benjamini-Hochberg FDR correction.

Western blotting and immunofluorescence. Western blotting was performed on up to 20 µg of the cell lystes that were used for proteomic analysis (above). Proteins were separated by SDS-PAGE using a 4-15% Tris-HCl Ready Gel (Bio-Rad). The following primary antibodies were used at 1:1000 dilution in 5% milk, including: GAPDH (Millipore MAB374), RSPH4A (Sigma-Aldrich HPA031196), repetin (Sigma-Aldrich HPA030483), TGM1 (Sigma-Aldrich HPA040171), keratin 6 (Thermo PA5-28235), keratin 14 (Novus 34270) and keratin 17 (Cell Signaling 12509). The following secondary antibodies were used at 1:3000 dilution in 5% milk: goat anti-rabbit HRP (Santa Cruz Biotech sc-2004) and goat anti-mouse HRP (Santa Cruz Biotech sc-2005).

Targeted quantitation of phosphorylated keratin 6. Stable isotope-labeled (SIL) peptides (SpikeTides L) were purchased from JPT and reconstituted in 0.1 M AmBic w/ 20% (v/v) MeCN. After reconstitution, ~100 fmol of neat peptides were analyzed by LC-MS/MS as described above for phosphopeptides except that the UPLC separation used a 30 min gradient of 3-30% buffer B. MS/MS data was searched in Mascot, and Skyline was used to build a spectral library and assign precursor peaks. An inclusion list (precursor mass, charge state, retention time window) was exported from Skyline and used to generate a parallel reaction monitoring (PRM) assay {Gallien, 2012 #99}. For analysis of K6 peptides by PRM, samples were spiked with ~2 fmol/µl of SIL peptides. Analysis of 2 µl of each sample used a 30 min UPLC separation as above. The MS acquisition used the Q-Exactive Plus with the following MS2 parameters: resolution, 17,500; AGC target, 5E4; Max IT, 128 ms; Isolation width, 1 m/z resolution. Data was imported into Skyline, and peptides were assigned using the spectral library, retention times of neat SIL peptides, and/or site-determining fragment ions. Areas of native and SIL-labeled peptides were performed using non-interfering y-series fragment ions. Skyline files containing results of PRM analysis have been made public as part of the Panorama Targeted Proteomics data repository (panoramaweb.org).

RESULTS

Quantitative proteomic analysis of an in vitro model of diacetyl vapor exposure. In order to better understand the cellular changes and signaling events associated with chronic diacetyl exposure, we treated well-differentiated tracheobronchial epithelial cells (TBECs), from four healthy human donors, to three successive exposures of DA vapor (~1000 ppm for 1 h on days

0, 2 and 4) versus control, and we performed separate quantitative analyses of the proteomes and phosphoproteomes of whole cell lysates harvested two days after the last exposure (see Methods). Briefly, proteins were digested with trypsin, and phosphospeptides were enriched using titanium dioxide (TiO_2) resin. The unenriched proteomes and TiO_2-enriched phosphoproteomes were separately analyzed by gel-free, label-free liquid chromatography, tandem mass spectrometry (LC-MS/MS). Each analysis included injections of a pooled quality control (QC) sample, analyzed at the beginning, middle and end of each run block, to assess analytical reproducibility. The label-free quantitation utilized accurate mass and retention time alignment of each LC-MS/MS run, followed by area under-the-curve-quantitation of identified peptides. The proteome analysis used only 250 ng of peptide digests per sample and resulted in quantitation of approximately 23,039 unique peptides, corresponding to 3,389 proteins (Tables S2-S3). The phosphoproteome was enriched from 200 µg of peptide digests per sample, and analysis of ~20% of each sample post-enrichment yielded quantitative data for 5,673 unique phosphopeptides from ~2000 proteins (Table S5). Among the quantified phosphopeptides, there were 5,087 with at least one pSer, 663 with at least 1 pThr and 65 with at least one pTyr.

Hematoxylin and eosin (H&E) staining of TBEC cross-sections showed that DA exposure resulted in a range of pathological effects (Fig. 1). While all donors appeared to exhibit loss of cilia after DA vapor exposure, there appeared to be some variability in the severity of the injury and remodeling of the epithelium. Specifically, cells from donor 1 appeared to be poorly attached to the permeable support and exhibited loss of cell-cell contacts throughout the culture (Fig. 1A), whereas the defining characteristic from donors 2-4 was a thickened and somewhat dysplastic layer of cells that was mostly adhered to the permeable support (Fig. 1B-D). We sought to correlate changes in the proteomes and phosphoproteomes of the TBECs with these aberrant histological features, and we applied several filters to identify the proteins and phosphopeptides, and corresponding pathways, that were most altered after DA exposure.

Decreases in protein and phosphoprotein expression largely reflect injury to multicilated cells after DA exposure. We filtered the protein data (Table S4) to include proteins that: 1) were quantified by 2 or more peptides; 2) had a %CV of <30% for triplicate analyses of a QC pool; and 3) met an FDR-corrected p-value of <0.1 for DA versus PBS-only groups (paired t-test; see Methods). This analysis identified 809 proteins that were differentially expressed between DA and PBS groups, with ~300 that were lower based on two-dimensional hierarchical clustering of these data (Fig. 2A). Text mining identified a cluster of 89 downregulated proteins (cluster 7) that contained a large number of cilia-related proteins, including components of the cilia motor protein complex (axonemal dynein), intraflagellar transport proteins and radial spoke head proteins (Table S3). We further queried the extensive immunohistochemical analyses of lung sections in the Human Protein Atlas (http://www.proteinatlas.org/), and we found that many of these proteins are highly expressed in ciliated cells of human bronchi. We used these data to create a protein signature of DA vapor injury to the airway epithelium (Table 1).

A similar filtering of the phosphoproteome data using reproducibility and significance cutoffs identified 1306 phosphopeptides that were differentially expressed between DA and PBS groups (Table S6). Clustering these data showed that greater than half of the phosphopeptides were reduced after DA exposure (Fig. 2B). While we could not localize the injury phenotype to a specific cluster of phosphopeptides, sorting by fold change suggested that the majority of downregulated phosphopeptides were associated with the loss of cilia or injury to multiciliated cells. We further filtered on proteins which had 2 or more associated phosphopeptides that were >5-fold lower in DA- versus PBS-treated cells, and we used these data to assemble a complementary phosphoprotein signature of injury (Table 2). While we could not exclude the possibility that dysregulated phosphorylation was due to specific alterations in kinase or phosphatase activity, the overlap in the protein and phosphoprotein signatures (12 proteins; e.g.

RSPH4A, TP53BP1 and CA087) suggested that the decreases in phosphorylation mostly reflected parallel changes protein expression.

Radial spokehead homolog 4A (RSPH4A) was found in both the protein and phosphoprotein signatures and had a large number of unique, downregulated phosphopeptides (Table 2). RSHP4A is highly expressed in the cytoplasm and membranes of multiciliated cells of the human airway {Lindskog, 2014 #94} and is the core protein of the radial spoke head, a complex which has a role in mechanical transduction of cilia. As a validation of our injury signatures, we showed that RSPH4A expression was markedly reduced in total lysates (Fig. 3A) and in the ciliated cells lining the apical surface of the DA-exposed epithelium (Fig. 3B). Interestingly, RSPH4A staining was increased in the basal layer of cells of injured cells, which could suggest some capacity of these cultures for re-differentiation to a ciliated phenotype. More generally, these data establish signatures of DA vapor exposure that appear to reflect extensive injury to the multiciliated cells of the airway epithelium.

Markers of squamous differentiation are upregulated after DA exposure. We next analyzed the proteins that were increased in DA-treated cells to determine whether they might reveal a molecular basis for repair or regeneration processes. After filtering of the data (2 or more quantified peptides; %CV of <30 for replicate injections of the QC pool; and FDR-corrected p-value<0.1; Table S3), the most highly overexpressed proteins included: ECM1 (+8-fold), a extracellular matrix protein that localizes to the basement membrane of skin and to squamous epithelium {Uhlen, 2015 #114}; GDF15 (+7.5-fold), a member of the TGF-β superfamily that is thought to play an early role in response to lung injury; and sequestosome-1 (+5-fold), a negative regulator of autophagy. These proteins did not appear to belong to a single common pathway. However, squamous differentiation was suggested by the localization of numerous small proline-rich proteins (SPR1B, SPR2A, SPRR3) and protein-glutamine gamma-glutamyltransferase K (TGM1) to a branch of the cluster dendrogram (clusters 10-12; Fig. 2B); and these proteins were also among the mostly highly upregulated in DA- versus PBS-treated cells (Table S3). We noted that a number of other putative markers of squamous differentiation—including involucrin—were highly expressed in donors 2-4, and available data in the Human Protein Atlas also showed that most of these proteins are more highly expressed in squamous (versus respiratory) epithelial cells. These data formed the basis for a protein signature of squamous differentiation (Table 3) and appeared to be consistent with the H&E staining of donors 2-4 (Figs. 1B-D) versus donor 1 (Fig. 1A).

Although most of the proteins in the signature serve a structural role, there were several enzymes of note, including TGM1, 1-acylglycerol-3-phosphate O-acyltransferase (ABHD5) and sulfotransferase family cytosolic 2B member 1 (ST2B1). TGM1 crosslinks SPRs, keratins and other proteins, as well as ω-OH-(glucosyl)acylceramide (GlyAcylCer) within the cornified envelope, a protective layer produced below the plasma membrane of terminally differentiating stratified squamous epithelia. ABHD5 been implicated triacylglycerol metabolism upstream and formation of GlyAcylCer for utilization by TGM1. Finally, ST2B1 possesses cholesterol sulfotransferase activity and is expressed is epidermis with fillagrin, a marker of late squamous differentiation {Higashi, 2004 #98}; the product of this enzyme, cholesterol sulfate, is incorporated into the cornified envelope and its expression parallels that of TGM1. Collectively, these data suggest a role for squamous differentiation in the aberrant repair of the epithelium after DA exposure.

In comparison, only few of the upregulated phosphopeptides were obviously related to the squamous phenotype. Four phosphopeptides belonging to TGM1, and a single phosphopeptide each from SPR2A and late cornified envelope protein 3D, were highly upregulated after DA treatment (Table S6). A query of large-scale phosphoproteomic data in the Phosphosite database (www.phosphosite.org) also showed that except for TGM1, very few phosphorylation sites have

been identified in proteins associated with the squamous phenotype, including the small-proline rich proteins or epithelial proteases. While we could not define a phosphoprotein signature of squamous differentiation, there were a number of phosphoproteins that were represented by multiple upregulated phosphopeptides (Table S6). These included: sequestosome-1, which was also upregulated at the protein level; the basal cell cytokeratins 6 and 14; SLC6A14, an amino acid transporter expressed in the airway epithelium; and tristetraprolin (TTP), an mRNA-binding protein that has been shown to destabilize interleukin 8 mRNA in the airway epithelium.

We used western blotting to confirm the increased expression of TGM1, as well as repetin, a protein that is expressed very late in the differentiation process. Consistent with the proteomic analysis, TGM1 levels were higher in all four donors after DA treatment, while levels of repetin were only elevated in donors 2-4 (Fig. 4A). Immunofluorescence analysis of cross-sections further showed that TGM1 localized to the plasma membrane in DA-treated TBECs with qualitatively highest expression in the basal-most layer of cells (Fig. 4B). Immunofluorescence also showed an increase in repetin levels in DA-exposed cells (Fig. 4C). In contrast to TGM1, repetin was not highly expressed in the basal layer of cells, which suggests that these cells are not fully committed to squamous differentiation. Collectively, these data correlate the dysplastic phenotype observed by H&E staining with the expression of markers of squamous differentiation. In donor 1, the low expression of repetin and many other markers of differentiation (Table 3) suggests that these cells may have lost their capacity for proliferation or differentiation, and this appears to be consistent with the H&E staining, which showed extensive loss of cell-cell junctions throughout the culture, as well as separation from the permeable support (Fig. 1A).

Basal cell cytokeratins are crosslinked and hyperphosphorylated following diacetyl-induced injury. The squamous phenotype suggested a role for airway “progenitor” cells-types in the remodeling of the epithelium after DA injury. Among airway stem cells, basal cells, which are often characterized based on expression of cytokeratins, constitute a larger percentage of the human upper airway epithelium as compared to uteroglobin/CCSP-expressing clara cells, and basal cells can also express many of the proteins that we have associated with the squamous phenotype. Our proteomic analysis quantified numerous “basal cell” keratins, including type II keratins 5 and 6 (K5 and K6) and type I keratins 14, 16 and 17 (K14, K16 and K17), in addition to CCSP. We wondered whether our proteomic data might provide better quantitation of the overall fate of airway progenitor cells in this model. In donor 1, which had low levels of squamous differentiation markers, all basal cell keratins were unchanged or lower after DA treatment (Fig. 5A), suggesting that basal cells might be lower in this donor after injury. In the other three donors, K6, K14, K16 and K17 were all increased after DA treatment (Fig. 4A), which could be a consequence of basal cell proliferation and/or squamous differentiation. On the other hand, CCSP was reduced in all DA-treated TBECs, suggesting a loss of clara cells in this model.

We used western blotting to independently validate the relative levels of a number of basal cell keratins. These data showed mostly lower levels of keratin monomers in DA-exposed donor 1 cells, but interestingly, DA treatment appeared to result in extensive crosslinking of keratins, as reflected in shifts of K5, K14, K6 and K17 to higher molecular weights (of ~2 times or greater mass) with small overall changes in the levels of keratin monomers (Fig. 5B). The cross-linked species were detectable, but overall lower in TBECs from donor 1, which correlated with the lower expression of basal keratins and squamous differentiation markers (including repetin) in these cells. Keratin crosslinking was also consistent with the increased expression of TGM1 throughout the basolateral layer of cells exposed to DA vapor (Fig. 4B). Transglutaminase mediated crosslinking of K5 and K6 to the cornified envelope has been previously demonstrated by mass spectrometry {Candi, 1998 #44}, although to our knowledge, transglutaminase-dependent crosslinking of type I keratins (i.e. K14 and K17) has not been previously shown. These data

suggest that the increased levels of basal and cytokeratins, as measured by the proteomic analysis, reflect an overall increase in total (monomer and crosslinked) keratins.

Within the phosphoproteome dataset, ~100 unique phosphopeptides were assigned to basal cell keratins (Table S6), of which almost ~40 peptides were differentially expressed between the DA and control groups. K6 and K14 phosphopeptides were most over-represented, and an overlay of these peptides onto the keratin protein sequences showed that a majority of the quantified phosphorylation sites were within the head and tail domains (Fig. S3), whereas we obtained high sequence coverage of non-phosphorylated peptides across the entire protein sequences (except for the Gly-rich region of the keratin head domain; Fig. S3). These data suggest that the disordered head and tail domains may be more accessible to kinases than the central alpha-helical rod domain and are also consistent with previously characterized phosphorylation sites on K8 and K18.

Based on their high differential expression in DA-treated versus control cells, we selected several of the K6 phosphopeptides for further validation using parallel reaction monitoring (PRM), a sensitive and precise targeted proteomic approach (see Methods). We focused primarily on a region in K6 between amino acids 18-60 that contained 12 total Ser residues, 9 of which were putatively phosphorylated in our dataset (Table S6 and Fig. S2). For targets that contained multiple phosphorylatable Ser residues, we assigned sites of phosphorylation using MS/MS fragment ions. The retention time and fragmentation of authentic stable isotope-labeled (SIL) standards were used to assign site localization of native K6 phosphopeptides containing a single phosphorylation site (Fig. 6A-B). Finally, enriched phosphopeptides from DA- versus PBS-treated cells were spiked with SIL standards and analyzed using PRM. Multiply phosphorylated peptides were quantified using a label-free approach, whereas singly phosphorylated peptides were normalized to internal standards, and ratios were calculated for DA versus PBS samples (Fig. 6C). Phosphopeptides with either pSer19/pSer22, pSer34/pSer37 or pSer44, were highly upregulated in all donors. Phosphopeptides with pSer19, pSer31 and pSer37 were >2-fold upregulated in donors 2-4, but unchanged or lower in donor 1, which resembled the pattern seen for K6 protein, and other squamous markers. Collectively, these data identify and establish quantitative assays for multiple previously uncharacterized phosphorylation sites in K6 that may be important for unraveling the pathophysiology of flavoring-induced epithelial injury.

DISCUSSION

Exposure to diacetyl has been implicated both clinically and experimentally in BO. Our work and that of others suggests early epithelial injury is a critical step in the process leading to airway fibrosis. Here, using proteomic analysis, we have been able to tease out distinct cellular events that occur in response to repeated DA vapor exposures of organotypic cultures of primary human airway cells. Our results are striking, both histologically and biologically, and they suggest an orderly series of changes in the epithelium originating in injury of multiciliated cells and progressing to repair/regeneration by basal cells, albeit with some variability across the cells from four individual donors.

The air-liquid interface culture has been vital for modeling epithelial injury and repair after exposure to environmental toxicants and respiratory pathogens. While there have been a number of proteomic analyses of differentiated TBEC secretions, to our knowledge, there has been only one prior study of the whole cell proteome of differentiated TBECs using mass-spectrometry based proteomics. With newer-generation technology, we have achieved a much greater depth of coverage (7-fold more total proteins quantified; 10-fold more proteins quantified by 2+ peptides), and for the first time, we have performed an integrated analysis of the proteomes and phosphoproteomes of differentiated TBECs. Still, the ease at which thousands of proteins and

phosphosites can be quantified belies the complexity of this model which is composed of as many as four distinct cell-types (basal, clara, goblet, multiciliated). The availability of validated antibodies (and cell and tissue-specific expression data)—a significant contribution of the Human Protein Atlas project—has allowed us to localize differentially-expressed proteins within the epithelium and to begin understand the significance of these changes. Although our data provides the first catalogue of potential regulatory phosphorylation sites in the human airway epithelium, complementary tools (e.g. targeted proteomic assays or phosphorylation site-specific antibodies) will needed to better understand their (patho)physiological functions.

The loss of cilia observed in our current study is consistent with in vivo models of flavoring-induced BO, as characterized by H&E staining of airways and transcriptomics of affected epithelium. More generally, loss of cilia is seen in epithelial injury by numerous other toxicants, including nitrogen dioxide, sulfur dioxide and naphthalene. Nonetheless, no models to date have clearly define this process on a proteome-wide scale. We have shown that (phospho)proteomic analysis can be used to measure many hundreds of proteins and phosphoproteins related to multiciliated cell structure/function; other relevant PTMs, including ubiquitinylation or acetylation, could be similarly quantified. It stands to reason that these techniques could be applied longitudinally in this model to better characterize the injury process, identify targets for therapeutic intervention and to better establish markers of epithelial injury that could be assessed in human cohorts.

There is a long-held view that the airway basal cell has significant plasticity for differentiation to a normal mucociliary or to a terminal squamous phenotype. One interpretation of our data might be that following initial injury, basal cells proliferate and undergo squamous differentiation (supported by evidence in at least three of the donors). In addition, all donors have markedly elevated levels of ECM1, a protein expressed in non-keratinized squamous epithelium of the esophagus and tonsil. These data and are last partially consistent with observations of squamous metaplasia and keratinization in rodent models of DA exposure; and interestingly, TGM1 was also among the highest upregulated transcripts in affected epithelia from lungs of PD-treated rats. While there are pathological implications (see below), these data also raise the question of how we might shift the differentiation process toward formation of a normal, healthy epithelium. Studies of basal cell differentiation have identified a number of mediators of mucociliary versus squamous differentiation, including vitamins A and D, epidermal growth factor, and pro-inflammatory cytokines. It will be of interest to determine whether targeting any of these soluble mediators, or their receptors, can attenuate aberrant epithelial repair after flavoring-induced injury, either in vitro or in vivo.

Our data describe several novel modifications to basal cell keratins. These proteins are often used for labeling, subtyping and/or lineage tracing of airway progenitor/stem cells, but relatively little attention has been paid to the role of post-translational modification of keratins in airway injury and/or repair. Among the crosslinked keratins, K17 is a particularly attractive candidate marker of squamous differentiation and cornified envelope formation, since it is highly expressed in basal cells of human bronchi and appears only to exist in its monomeric form under normal conditions. The pathophysiological implications of keratin phosphorylation are less well understood but have been observed to occur during mitosis or upon activation of stress-dependent kinases. Additional studies will be required to fully understand the role of K6 phosphorylation in flavoring-induced injury, but our results thus far identify numerous phosphopeptides that may serve as potential markers of epithelial injury, including several that were barely detectable in PBS controls. While the spatial localization of these modified keratins cannot as yet be determined, the methodologies presented here should be applicable to the study of human airway biopsies (or explanted/postmortem tissue); and using rat keratin-specific

standards, it would be straightforward to develop targeted assays to probe for K6 phosphorylation in the well-studied in vivo models of flavoring-induced BO.

Conclusions: Diacetyl-exposed cells showed a marked reduction in proteins and phosphopeptides related to cilia structure-function, and extensive injury to ciliated cells was confirmed by staining of airway culture sections. Conversely, a protein signature of squamous metaplasia was markedly elevated following diacetyl exposure. This signature correlated with apparent transglutaminase-mediated crosslinking of basal cell cytokeratins and the suprabasal expression of repetin, a marker of terminal squamous differentiation. Diacetyl vapor exposure also led to large increases in phosphorylation of previously uncharacterized sites in the head and tail domains of cytokeratins K6 and K14. Collective, these results suggest that basal cell differentiation, and squamous metaplasia, may represent a precursor to flavoring-induced BO and identify specific cellular markers at a protein level useful to screen at risk workers.

Publications:

1. Proteomic analysis of primary human airway epithelial cells after in vitro exposure to diacetyl vapor. [2017] Matthew W. Foster[1,2], William M. Gwinn[3], Francine L. Kelly[1], David M. Brass[1], J. Will Thompson[2], M. Arthur Moseley[2], Daniel L. Morgan[3] and Scott M. Palmer. **(in press Journal of Proteome Research)**

2. Secretome analysis of human airway epithelium after diacetyl exposure reveals new insights into flavoring induced airways disease. [2017] David M. Brass, William M Gwinn, Ashlee M. Valente, Francine L. Kelly, Christie D. Brinkley, Andrew E. Nagler, M. Arthur Moseley, Dan Morgan, Scott M. Palmer and Matthew W. Foster. **(under review American Journal of Respiratory Cell and Molecular Biology)**

Human subjects Material – None or N/A

Material for other investigators - None

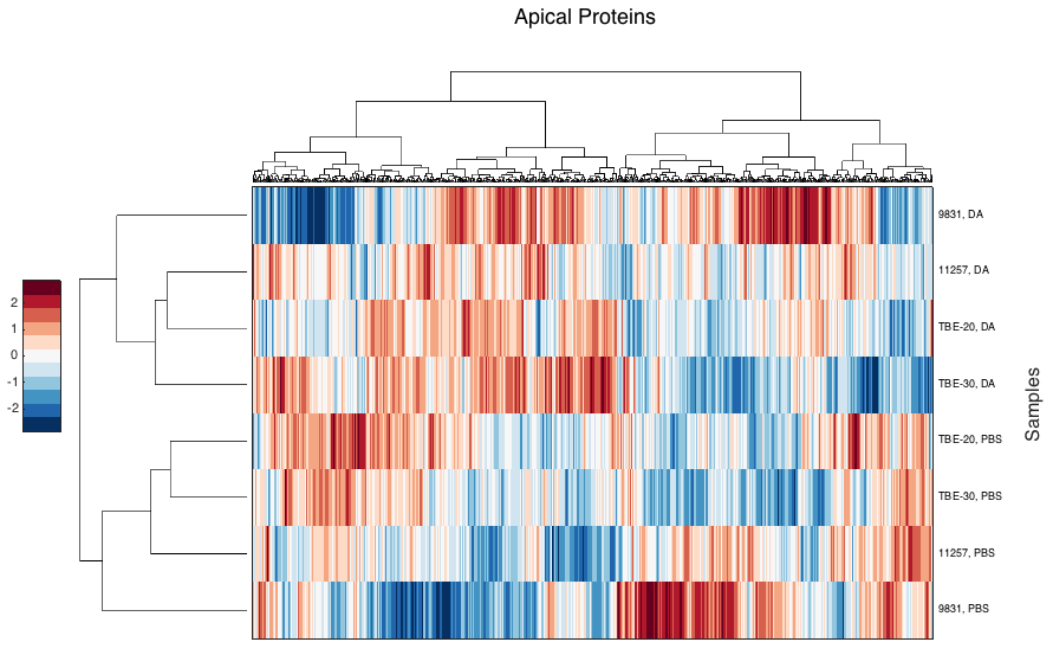
Apical Proteins
2
1
0
-1
-2
9831, DA
11257, DA
TBE-20, DA
TBE-30, DA
TBE-20, PBS
TBE-30, PBS
11257, PBS
9831, PBS
Samples

Fig 1

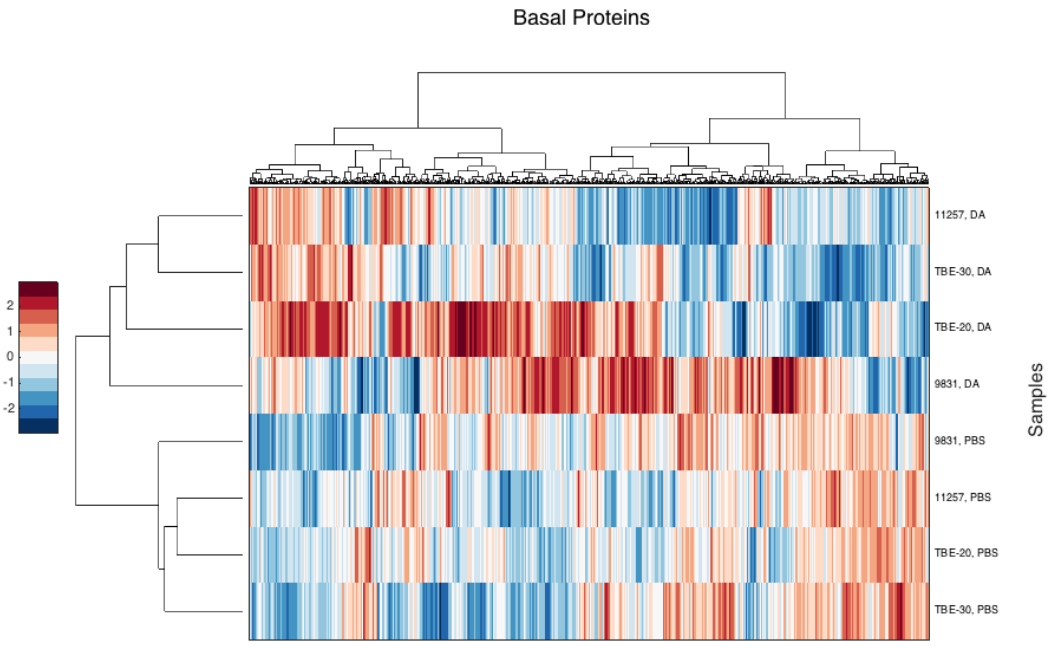
Basal Proteins
2
1
0
-1
-2
11257, DA
TBE-30, DA
TBE-20, DA
9831, DA
9831, PBS
11257, PBS
TBE-20, PBS
TBE-30, PBS
Samples

Fig 2

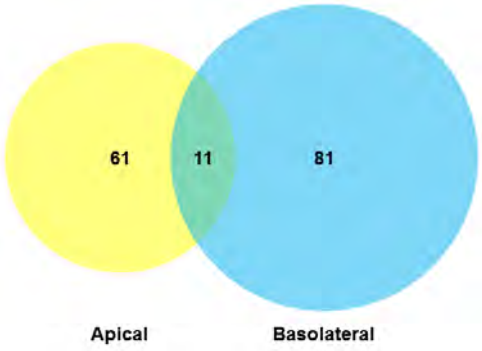

Figure 3. The apical and basolateral secretomes of DA-exposed primary human airway epithelial cells are highly polarized. The Venn diagram shows the overlap of differentially expressed protein sets, significant at the level of FDR < 0.1.

Figure 3 –

Table 1. Apical proteins with significantly altered expression in DA vs. PBS

Primary Protein Name	Protein Description	Peptide Count	%CV QC	Fold Change DA vs. PBS	t-test P-value	t-test P-value w/FDR Correction
KLK6_HUMAN	Kallikrein-related peptidase 6	4	6.7	7.0	0.004	0.068
ECM1_HUMAN	Extracellular matrix protein 1	7	19.9	6.8	0.010	0.089
H4_HUMAN	Histone cluster 4, H4	6	15.3	6.3	0.004	0.065
TRFE_HUMAN	Transferrin	11	17.2	4.7	0.002	0.054
H2B1M_HUMAN	Histone H2B type F-S	3	10.2	4.3	0.005	0.078
LAMA3_HUMAN	Laminin subunit alpha-3	13	18.4	4.0	0.007	0.080
DSC2_HUMAN	Desmocollin-2	2	15.3	3.9	0.003	0.065
DKK1_HUMAN	Dickkopf-related protein 1	2	9.5	3.6	0.002	0.054
H2AY_HUMAN	Core histone macro-H2A.1	4	6.2	3.3	0.011	0.091
CCD80_HUMAN	Coiled-coil domain-containing protein 80	2	2.2	3.0	0.001	0.054
FLNA_HUMAN	Filamin-A	12	14.3	2.8	0.008	0.085
LAMB3_HUMAN	Laminin subunit beta-3	9	11.7	2.7	0.004	0.065
MMP9_HUMAN	Matrix metalloproteinase-9	8	14.6	2.7	0.000	0.054
PGBM_HUMAN	Basement membrane-specific heparan sulfate proteoglycan core protein	15	5.6	2.6	0.006	0.080
LEG1_HUMAN	Galectin-1	3	27.6	2.6	0.011	0.095
CEAM6_HUMAN	Carcinoembryonic antigen-related cell adhesion molecule 6	5	17.0	2.5	0.008	0.083
LAMC2_HUMAN	Laminin subunit gamma-2	16	14.3	2.5	0.007	0.080
ST14_HUMAN	Suppressor of tumorigenicity 14 protein	2	7.6	2.3	0.010	0.086
GDF15_HUMAN	Growth/differentiation factor 15	4	19.6	2.2	0.002	0.054
PSB5_HUMAN	Proteasome subunit beta type-5	3	9.0	2.2	0.013	0.098
MMP10_HUMAN	Stromelysin-2	3	18.5	2.1	0.009	0.086
LYPD3_HUMAN	Ly6/PLAUR domain-containing protein 3	5	4.8	2.1	0.000	0.016
APLP2_HUMAN	Amyloid-like protein 2	2	1.6	2.0	0.001	0.054
RSMN_HUMAN	Small nuclear ribonucleoprotein-associated protein N	2	17.9	2.0	0.006	0.078
EPS8_HUMAN	Epidermal growth factor receptor kinase substrate 8	7	29.5	2.0	0.012	0.097
TENA_HUMAN	Tenascin C	11	7.4	1.9	0.002	0.054
DSG2_HUMAN	Desmoglein-2	5	10.3	1.9	0.003	0.065
PEPD_HUMAN	Xaa-Pro dipeptidase	3	27.8	1.8	0.002	0.054
SSBP_HUMAN	Single-stranded DNA-binding protein mitochondrial	4	6.6	1.8	0.009	0.086
TIMP1_HUMAN	Metalloproteinase inhibitor 1	5	8.5	1.8	0.009	0.086
CSTN1_HUMAN	Calsyntenin-1	5	5.0	1.7	0.002	0.054
PSA3_HUMAN	Proteasome subunit alpha type-3	3	7.4	1.6	0.010	0.086
ANXA8_HUMAN	Annexin A8	5	3.6	1.6	0.012	0.097
PSB6_HUMAN	Proteasome subunit beta type-6	3	10.9	1.6	0.012	0.097
PSA7_HUMAN	Proteasome subunit alpha type-7	7	1.4	1.5	0.005	0.078
TKT_HUMAN	Transketolase	13	8.3	1.5	0.007	0.080
CD14_HUMAN	Monocyte differentiation antigen CD14	3	4.7	1.5	0.005	0.078
CADH1_HUMAN	Cadherin-1	8	9.4	1.4	0.007	0.080
SPTN1_HUMAN	Spectrin alpha chain non-erythrocytic 1	25	3.1	1.4	0.013	0.098
PRDX1_HUMAN	Peroxiredoxin-1	14	3.3	1.3	0.009	0.086
SPTB2_HUMAN	Spectrin beta chain brain 1	10	12.5	1.3	0.007	0.080
GNAI2_HUMAN	Guanine nucleotide-binding protein G(i) alpha-2 subunit	3	1.2	1.1	0.009	0.086
PSA_HUMAN	Puromycin-sensitive aminopeptidase	11	13.7	-1.1	0.003	0.065
DDB1_HUMAN	DNA damage-binding protein 1	8	4.2	-1.2	0.002	0.058
SLPI_HUMAN	Antileukoproteinase	7	3.3	-1.4	0.009	0.086
CBX3_HUMAN	Chromobox protein homolog 3	2	3.5	-1.5	0.001	0.054
GELS_HUMAN	Gelsolin	31	6.7	-1.5	0.006	0.078
HSP71_HUMAN	Heat shock 70 kDa protein 1	6	5.4	-1.6	0.004	0.065
FUBP1_HUMAN	Far upstream element-binding protein 1	3	10.4	-1.7	0.012	0.097
AL1A1_HUMAN	Retinal dehydrogenase 1	15	7.9	-1.7	0.001	0.054
THIL_HUMAN	Acetyl-CoA acetyltransferase mitochondrial	2	24.5	-1.8	0.006	0.078
CFAB_HUMAN	Complement factor B	26	21.6	-1.8	0.003	0.065
S10A4_HUMAN	Protein S100-A4	2	12.6	-1.8	0.003	0.065
PEDF_HUMAN	Pigment epithelium-derived factor	15	8.4	-2.1	0.012	0.097
CD59_HUMAN	CD59 glycoprotein	4	6.4	-2.2	0.001	0.054
PIGR_HUMAN	Polymeric immunoglobulin receptor	36	7.4	-2.3	0.007	0.080
BPIA1_HUMAN	BPI fold-containing family A member 1	5	12.7	-2.4	0.007	0.080
PLTP_HUMAN	Phospholipid transfer protein	4	10.1	-2.6	0.002	0.054
FBLN3_HUMAN	EGF-containing fibulin-like extracellular matrix protein 1	14	12.1	-2.7	0.002	0.054
AACT_HUMAN	Alpha-1-antichymotrypsin	7	20.0	-3.4	0.004	0.065
MANBA_HUMAN	Beta-mannosidase	4	17.0	-3.4	0.006	0.078
B2MG_HUMAN	Beta-2-microglobulin	6	25.5	-3.5	0.001	0.054
NUCB2_HUMAN	Nucleobindin-2	5	19.5	-3.9	0.006	0.078
IBP7_HUMAN	Insulin-like growth factor-binding protein 7	10	10.6	-3.9	0.013	0.098
A1AT_HUMAN	Alpha-1-antitrypsin	7	6.9	-5.6	0.001	0.054
CEL_HUMAN	Bile salt-activated lipase	5	15.5	-5.6	0.002	0.056
CYTM_HUMAN	Cystatin-M	3	15.5	-5.9	0.001	0.054
IBP2_HUMAN	Insulin-like growth factor-binding protein 2	11	6.3	-6.5	0.005	0.078
CLUS_HUMAN	Clusterin	9	4.6	-11.0	0.001	0.054
ISK5_HUMAN	Serine protease inhibitor Kazal-type 5	2	8.6	-11.9	0.008	0.086
CO4A_HUMAN	Complement C4-A	5	7.4	-14.8	0.002	0.057
CDHR3_HUMAN	Cadherin-related family member 3	3	5.3	-20.7	0.002	0.056

Table 2. Basolateral proteins with significantly altered expression in DA vs. PBS

Primary Protein Name	Protein Description	Peptide Count	%CV QC	Fold Change DA vs. PBS	t-test P-value	t-test P-value w/FDR Correction
A2ML1_HUMAN	Alpha-2-macroglobulin-like protein 1	7	16.6	11.9	0.011	0.099
UPAR_HUMAN	Urokinase plasminogen activator surface receptor	3	26.2	10.5	0.009	0.095
ECM1_HUMAN	Extracellular matrix protein 1	24	10.5	9.9	0.001	0.061
PRS27_HUMAN	Serine protease 27	3	11.1	9.2	0.011	0.099
DAF_HUMAN	Complement decay-accelerating factor	4	3.1	8.8	0.008	0.094
EPHA2_HUMAN	Ephrin type-A receptor 2	6	15.1	6.4	0.001	0.061
TIMP1_HUMAN	Metalloproteinase inhibitor 1	5	7.0	5.7	0.001	0.067
ZG16B_HUMAN	Zymogen granule protein 16 homolog B	3	12.7	5.2	0.003	0.083
PCDGK_HUMAN	Protocadherin gamma-C3	2	9.8	4.6	0.010	0.099
GOLM1_HUMAN	Golgi membrane protein 1	8	4.2	4.5	0.005	0.090
IL36G_HUMAN	Interleukin-36 gamma	3	10.3	4.5	0.008	0.094
BSSP4_HUMAN	Brain-specific serine protease 4	4	12.4	4.5	0.001	0.067
DNJA4_HUMAN	DnaJ homolog subfamily A member 4	2	13.0	4.4	0.003	0.083
MARCS_HUMAN	Myristoylated alanine-rich C-kinase substrate	8	10.5	4.2	0.003	0.083
CAP1_HUMAN	Adenylyl cyclase-associated protein 1	7	2.3	4.1	0.008	0.094
VASN_HUMAN	Vasorin	7	2.8	4.0	0.010	0.099
PSCA_HUMAN	Prostate stem cell antigen	3	10.5	4.0	0.002	0.075
NRP1_HUMAN	Neuropilin-1	3	24.1	4.0	0.006	0.094
DDAH1_HUMAN	N(G) N(G)-dimethylarginine dimethylaminohydrolas	4	13.8	3.8	0.003	0.083
KLK10_HUMAN	Kallikrein-10	6	15.8	3.7	0.005	0.093
BASP1_HUMAN	Brain acid soluble protein 1	10	11.3	3.7	0.003	0.083
CXL16_HUMAN	C-X-C motif chemokine 16	2	10.8	3.6	0.005	0.090
EFNB1_HUMAN	Ephrin-B1	4	16.5	3.6	0.004	0.090
PCDH1_HUMAN	Protocadherin-1	13	9.3	3.6	0.000	0.061
GPX3_HUMAN	Glutathione peroxidase 3	5	9.0	3.4	0.009	0.099
VSIG2_HUMAN	V-set and immunoglobulin domain-containing protei	2	5.6	3.4	0.008	0.094
S100P_HUMAN	Protein S100-P	4	8.0	3.4	0.007	0.094
EPCR_HUMAN	Endothelial protein C receptor	4	10.4	3.3	0.011	0.099
GRN_HUMAN	Granulins	12	6.9	3.3	0.000	0.008
LAYN_HUMAN	Layilin	6	2.0	3.2	0.001	0.068
CATD_HUMAN	Cathepsin D	14	6.7	3.2	0.003	0.083
GDF15_HUMAN	Growth/differentiation factor 15	11	11.0	3.2	0.001	0.067
TIMP2_HUMAN	Metalloproteinase inhibitor 2	8	10.4	3.1	0.004	0.090
LRRF1_HUMAN	Leucine-rich repeat flightless-interacting protein 1	3	6.8	3.1	0.007	0.094
VIME_HUMAN	Vimentin	8	10.4	3.0	0.001	0.061
SPIT1_HUMAN	Kunitz-type protease inhibitor 1	27	7.0	3.0	0.003	0.083
SEM7A_HUMAN	Semaphorin-7A	6	15.9	3.0	0.000	0.004
PIP_HUMAN	Prolactin-inducible protein	9	15.7	2.9	0.006	0.094
CATB_HUMAN	Cathepsin B	17	11.7	2.7	0.001	0.070
SPIT2_HUMAN	Kunitz-type protease inhibitor 2	2	15.3	2.6	0.001	0.067
APLP2_HUMAN	Amyloid-like protein 2	8	10.5	2.5	0.007	0.094
MMP14_HUMAN	Matrix metalloproteinase-14	5	9.5	2.3	0.011	0.099
DIAC_HUMAN	Di-N-acetylchitobiase	5	17.9	2.3	0.008	0.094
PNPH_HUMAN	Purine nucleoside phosphorylase	5	26.0	2.3	0.011	0.099
QSOX1_HUMAN	Sulfhydryl oxidase 1	18	3.9	2.2	0.002	0.075
RBSK_HUMAN	Ribokinase	2	16.7	2.2	0.001	0.061
TXND5_HUMAN	Thioredoxin domain-containing protein 5	7	6.4	2.1	0.011	0.099
MMP9_HUMAN	Matrix metalloproteinase-9	16	10.6	2.1	0.010	0.099
A4_HUMAN	Amyloid beta A4 protein	13	19.6	2.0	0.003	0.083
HEBP2_HUMAN	Heme-binding protein 2	9	9.4	2.0	0.003	0.083
CAH13_HUMAN	Carbonic anhydrase 13	2	19.9	2.0	0.002	0.072
CYTB_HUMAN	Cystatin-B	10	11.6	1.9	0.005	0.092
TRXR1_HUMAN	Thioredoxin reductase 1 cytoplasmic	5	19.6	1.9	0.010	0.099
TRFE_HUMAN	Serotransferrin	36	5.8	1.8	0.002	0.082
CPPED_HUMAN	Calcineurin-like phosphoesterase domain-containing	4	23.6	1.8	0.007	0.094
DDR1_HUMAN	Epithelial discoidin domain-containing receptor 1	9	9.2	1.8	0.008	0.094
NEO1_HUMAN	Neogenin	8	5.6	1.8	0.010	0.099
GDIR2_HUMAN	Rho GDP-dissociation inhibitor 2	2	24.7	1.7	0.007	0.094
AATM_HUMAN	Aspartate aminotransferase mitochondrial	15	11.6	1.7	0.011	0.099
GLRX1_HUMAN	Glutaredoxin-1	3	12.0	1.7	0.008	0.094
K22E_HUMAN	Keratin type II cytoskeletal 2 epidermal	10	3.7	1.7	0.006	0.094
SPTB2_HUMAN	Spectrin beta chain brain 1	7	12.9	1.6	0.011	0.099
PSB6_HUMAN	Proteasome subunit beta type-6	4	6.0	1.4	0.011	0.099
PSB1_HUMAN	Proteasome subunit beta type-1	4	25.7	1.2	0.001	0.068
THOP1_HUMAN	Thimet oligopeptidase	4	5.7	-1.3	0.009	0.094
ACPH_HUMAN	Acylamino-acid-releasing enzyme	7	8.7	-1.4	0.006	0.094
PTPRF_HUMAN	Receptor-type tyrosine-protein phosphatase F	14	9.9	-1.7	0.005	0.090
ADH7_HUMAN	Alcohol dehydrogenase class 4 mu/sigma chain	18	8.6	-1.9	0.007	0.094
DDB1_HUMAN	DNA damage-binding protein 1	13	9.8	-1.9	0.003	0.083
HIBCH_HUMAN	3-hydroxyisobutyryl-CoA hydrolase mitochondrial	3	5.6	-2.1	0.005	0.090
INO1_HUMAN	Inositol-3-phosphate synthase 1	3	4.6	-2.2	0.007	0.094
BCAM_HUMAN	Basal cell adhesion molecule	14	8.7	-2.2	0.007	0.094
H2A1B_HUMAN	Histone H2A type 1-B/E	6	9.0	-2.9	0.007	0.094
RCC2_HUMAN	Regulator of chromosome condensation 2	10	9.2	-3.1	0.006	0.094
RNAS4_HUMAN	Ribonuclease 4	3	2.6	-3.3	0.006	0.094
FBLN3_HUMAN	EGF-containing fibulin-like extracellular matrix prote	12	8.9	-3.4	0.008	0.094
GLNA_HUMAN	Glutamine synthetase	6	15.9	-3.6	0.007	0.094
EGFR_HUMAN	Epidermal growth factor receptor	3	10.0	-3.7	0.004	0.090
GPNMB_HUMAN	Transmembrane glycoprotein NMB	3	9.5	-3.7	0.004	0.090
CO7A1_HUMAN	Collagen alpha-1(VII) chain	8	14.2	-3.8	0.009	0.094
CO5A2_HUMAN	Collagen alpha-2(V) chain	2	23.6	-3.9	0.005	0.090
LEG7_HUMAN	Galectin-7	13	10.3	-3.9	0.011	0.099
CO1A1_HUMAN	Collagen alpha-1(I) chain	3	9.8	-4.1	0.009	0.094
PHYD1_HUMAN	Phytanoyl-CoA dioxygenase domain-containing prot	2	17.0	-4.1	0.006	0.094
C1S_HUMAN	Complement C1s subcomponent	2	2.5	-4.1	0.003	0.083
C1R_HUMAN	Complement C1r subcomponent	7	6.1	-4.2	0.002	0.082
EPHB2_HUMAN	Ephrin type-B receptor 2	5	2.5	-4.2	0.001	0.067
LMNB2_HUMAN	Lamin-B2	7	24.0	-4.7	0.008	0.094
IBP7_HUMAN	Insulin-like growth factor-binding protein 7	22	13.8	-5.0	0.000	0.008
XRCC6_HUMAN	X-ray repair cross-complementing protein 6	2	11.6	-6.2	0.004	0.089
CELR1_HUMAN	Cadherin EGF LAG seven-pass G-type receptor 1	2	9.8	-17.4	0.012	0.099
IMPA2_HUMAN	Inositol monophosphatase 2	2	11.8	-31.9	0.001	0.067

Table 3. Basolateral proteins with significantly altered apical and basolateral expression in common DA vs. PBS

Primary Protein Name	Protein Description	Apical Fold Change DA vs. PBS	Basolateral Fold Change DA vs. PBS
ECM1_HUMAN	Extracellular matrix protein 1	6.756	10.988
TRFE_HUMAN	Serotransferrin	4.687	1.950
MMP9_HUMAN	Matrix metalloproteinase-9	2.690	2.415
GDF15_HUMAN	Growth/differentiation factor 15	2.230	2.623
APLP2_HUMAN	Amyloid-like protein 2	2.029	1.970
TIMP1_HUMAN	Metalloproteinase inhibitor 1	1.801	4.957
PSB6_HUMAN	Proteasome subunit beta type-6	1.560	1.185
SPTB2_HUMAN	Spectrin beta chain brain 1	1.277	1.421
DDB1_HUMAN	DNA damage-binding protein 1	-1.182	-2.027
FBLN3_HUMAN	EGF-containing fibulin-like extracellular matrix protein 1	-2.738	-2.818
IBP7_HUMAN	Insulin-like growth factor-binding protein 7	-3.910	-5.367

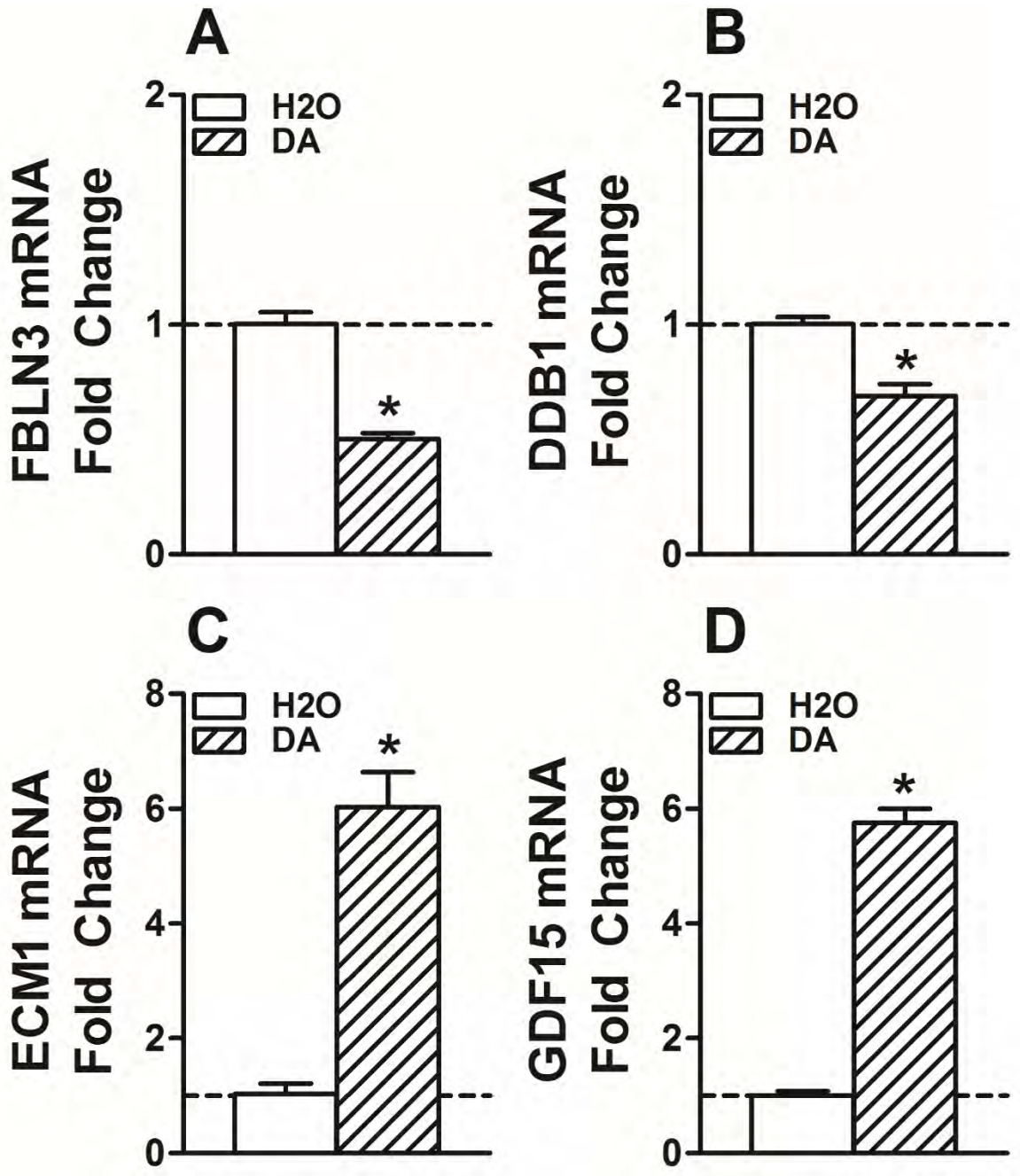
A
B
C
D
H2O
DA
FBLN3 mRNA
Fold Change
DDB1 mRNA
Fold Change
ECM1 mRNA
Fold Change
GDF15 mRNA
Fold Change
0
1
2
4
6
8
*

Figure 4

Table 4: Top 10 REACTOME Pathways enriched in proteins upregulated in Apical by DA exposure					
Pathway Name	**# Proteins**	**# Proteins in Pathway**	**p-value**	**FDR**	**Proteins Identified**
Degradation of the extracellular matrix	8	135	1.28E-07	5.43E-05	LAMC2; CADH1; LAMA3; MMP10; LAMB3; PGBM; MMP9; TIMP1
Extracellular matrix organization	10	291	4.37E-07	7.68E-05	LAMC2; CADH1; CEAM6; LAMA3; MMP10; LAMB3; PGBM; MMP9;
Apoptosis	8	165	5.80E-07	7.68E-05	CADH1; PSA3; DSG2; CD14; PSB6; PSA7; PSB5; SPTN1
Programmed Cell Death	8	170	7.24E-07	7.68E-05	CADH1; PSA3; DSG2; CD14; PSB6; PSA7; PSB5; SPTN1
Cell-Cell communication	7	139	2.48E-06	2.08E-04	LAMC2; CADH1; LAMA3; LAMB3; SPTB2; SPTN1; FLNA
Non-integrin membrane-ECM interactions	5	59	6.51E-06	4.56E-04	LAMC2; LAMA3; LAMB3; PGBM; TENA
Laminin interactions	4	30	1.01E-05	6.08E-04	LAMC2; LAMA3; LAMB3; PGBM
Type I hemidesmosome assembly	3	11	1.73E-05	9.15E-04	LAMC2; LAMA3; LAMB3
TCF dependent signaling in response to WNT	7	198	2.44E-05	1.00E-03	PSA3; H2B1M; H4; PSB6; PSA7; DKK1; PSB5
Anchoring fibril formation	3	15	4.32E-05	1.00E-03	LAMC2; LAMA3; LAMB3
Cell junction organization	5	90	4.86E-05	1.00E-03	LAMC2; CADH1; LAMA3; LAMB3; FLNA

Table 4

Table 5: Top 10 REACTOME Pathways enriched in proteins downregulated in Apical by DA exposure					
Pathway name	**# Proteins**	**# Proteins in Pathway**	**p-value**	**FDR**	**Proteins Identified**
Regulation of Complement cascade	3	27	9.74E-05	9.74E-03	CFAB; CD59; CO4A
Activation of C3 and C5	2	7	2.49E-04	1.25E-02	CFAB; CO4A
Lipid digestion, mobilization, and transport	3*	70	1.54E-03	4.95E-02	PLTP; CEL
HDL-mediated lipid transport	2*	20	1.98E-03	4.95E-02	PLTP
Complement cascade	4	201	4.00E-03	5.49E-02	CLUS; CFAB; CD59; CO4A
Platelet degranulation	3	105	4.82E-03	5.49E-02	A1AT; CLUS; AACT
Lipoprotein metabolism	2*	32	4.95E-03	5.49E-02	PLTP
Cargo concentration in the ER	2	33	5.25E-03	5.49E-02	A1AT; CD59
Response to elevated platelet cytosolic Ca2+	3	110	5.49E-03	5.49E-02	A1AT; CLUS; AACT
Utilization of Ketone Bodies	1	3	9.75E-03	8.77E-02	THIL
Lysosomal oligosaccharide catabolism	1	4	1.30E-02	1.03E-01	MANBA
*NB: PLTP has two natural variants					

Table 5

Table 6: Top 10 REACTOME Pathways enriched in proteins upregulated in Basolateral by DA exposure					
Pathway name	**# Proteins**	**# Proteins in Pathway**	**p-value**	**FDR**	**Proteins Identified**
Platelet degranulation	7	105	7.24E-06	1.90E-03	ECM1; QSOX1; CAP1; TIMP1; APLP2; A4; TRFE
Response to elevated platelet cytosolic Ca2+	7	110	9.77E-06	1.90E-03	ECM1; QSOX1; CAP1; TIMP1; APLP2; A4; TRFE
Activation of Matrix Metalloproteinases	4	32	6.98E-05	9.07E-03	TIMP2; MMP14; MMP9; TIMP1
Degradation of the extracellular matrix	6	135	3.06E-04	2.97E-02	CATB; TIMP2; CATD; MMP14; MMP9; TIMP1
Signaling by MST1	2	5	5.47E-04	4.27E-02	SPIT2; SPIT1
Extracellular matrix organization	8	291	7.46E-04	4.85E-02	CATB; TIMP2; CATD; MMP14; DDR1; MMP9; TIMP1; A4
Collagen degradation	4	63	8.97E-04	4.93E-02	CATB; CATD; MMP14; MMP9
Platelet activation, signaling and aggregation	7	256	1.68E-03	8.05E-02	ECM1; QSOX1; CAP1; TIMP1; APLP2; A4; TRFE
Axon guidance	10	551	3.67E-03	1.58E-01	EPHA2; NEO1; PSB1; PSB6; CAP1; SPTB2; EFNB1; NRP1; MMP9; SEM7A
EPH-ephrin mediated repulsion of cells	3	50	4.79E-03	1.87E-01	EPHA2; EFNB1; MMP9

Table 6

Table 7: Top 10 REACTOME Pathways enriched in proteins downregulated in Basolateral by DA exposure					
Pathway name	**# Proteins**	**# Proteins in Pathway**	**p-value**	**FDR**	**Proteins Identified**
PTK6 promotes HIF1A stabilization	2	6	1.49E-04	4.54E-02	GPNMB; EGFR
Synthesis of IP2, IP, and Ins in the cytosol	2	11	4.97E-04	4.83E-02	IMPA2; INO1
Assembly of collagen fibrils and other multimeric structures	3	55	5.71E-04	4.83E-02	CO5A2; CO7A1; CO1A1
Collagen degradation	3	63	8.45E-04	4.83E-02	CO5A2; CO7A1; CO1A1
Anchoring fibril formation	2	15	9.18E-04	4.83E-02	CO7A1; CO1A1
Collagen biosynthesis and modifying enzymes	3	66	9.66E-04	4.83E-02	CO5A2; CO7A1; CO1A1
Integrin cell surface interactions	3	86	2.06E-03	8.34E-02	CO5A2; CO7A1; CO1A1
Collagen formation	3	88	2.19E-03	8.34E-02	CO5A2; CO7A1; CO1A1
Syndecan interactions	2	27	2.91E-03	9.60E-02	CO5A2; CO1A1
Signaling by Overexpressed Wild-Type EGFR in Cancer	1	2	5.88E-03	1.59E-01	EGFR

Table 7

Supplementary Figures

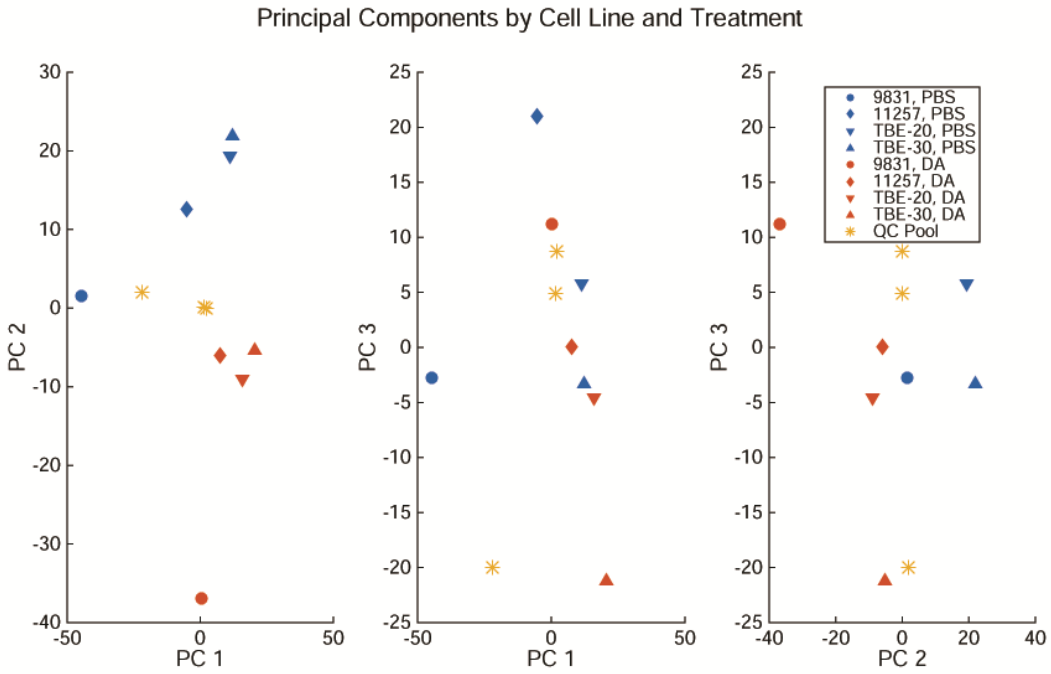

Figure S1 PCA Apical

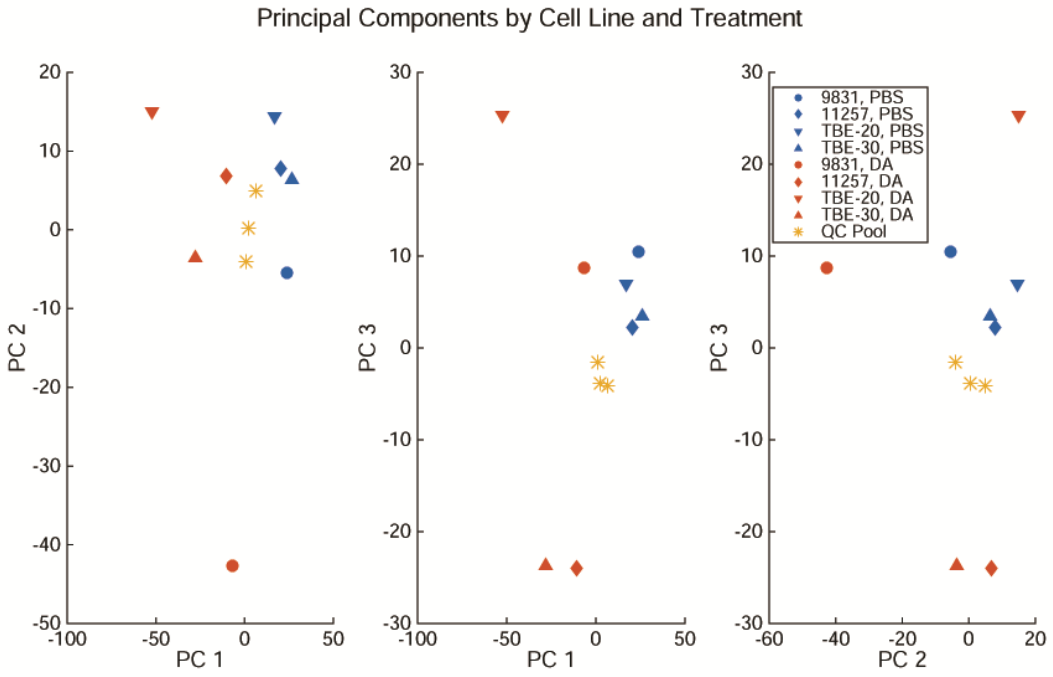

Figure S2 PCA Basolateral

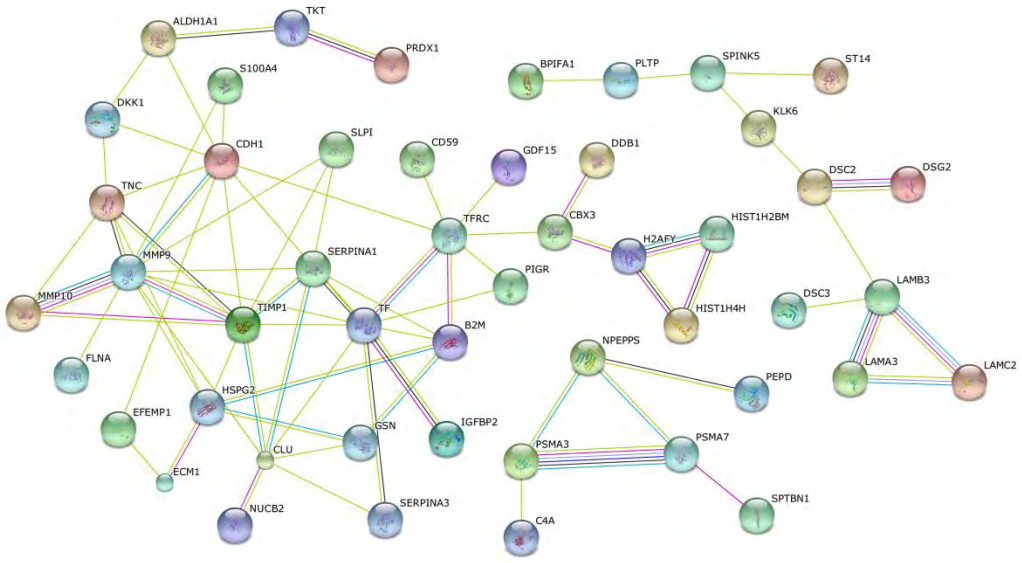

Figure S3 Apical String

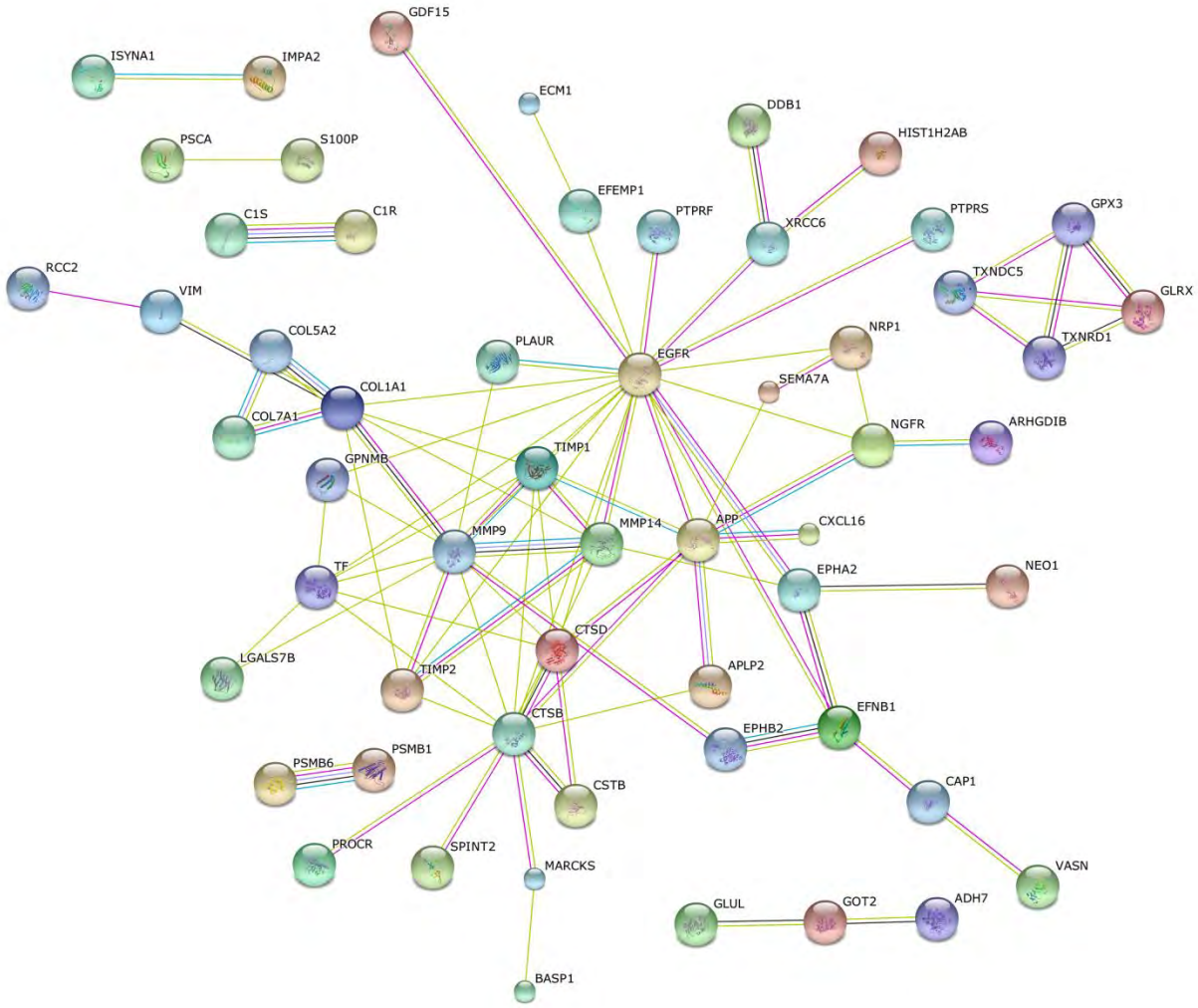

Figure S4 Basolateral String

Figure 1

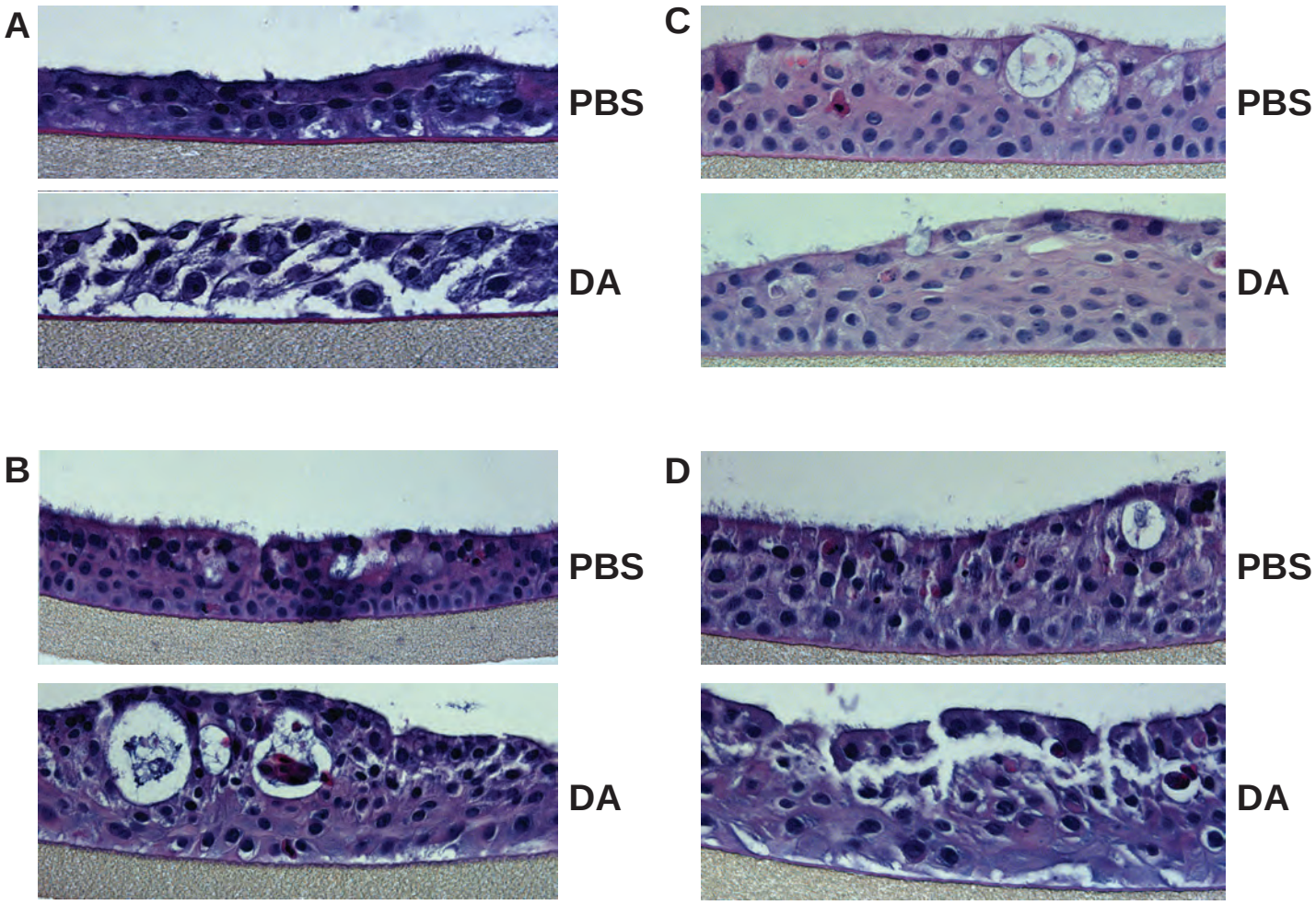

Figure 2

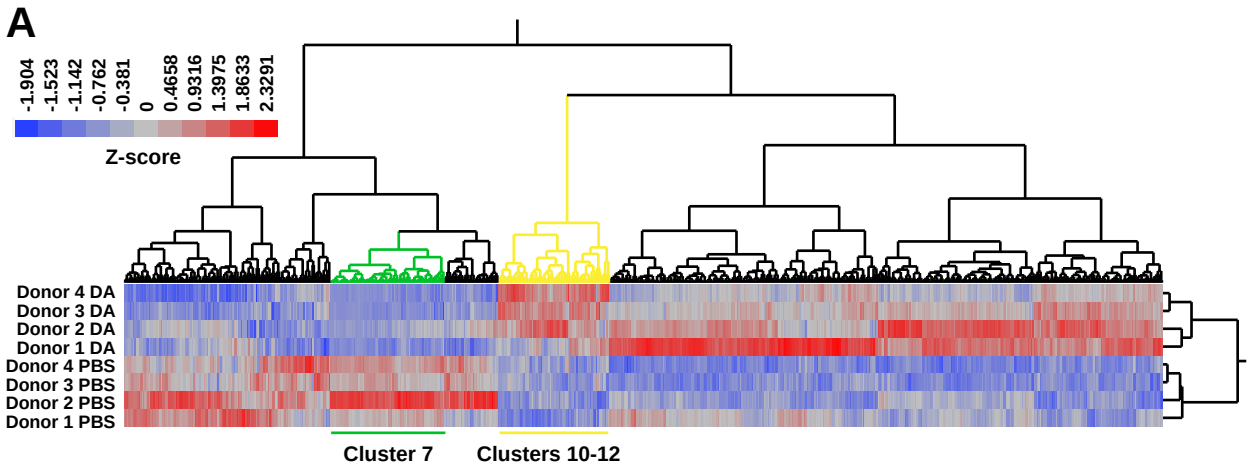
A
-1.904
-1.523
-1.142
-0.762
-0.381
0
0.4658
0.9316
1.3975
1.8633
2.3291
Z-score
Donor 4 DA
Donor 3 DA
Donor 2 DA
Donor 1 DA
Donor 4 PBS
Donor 3 PBS
Donor 2 PBS
Donor 1 PBS
Cluster 7
Clusters 10-12

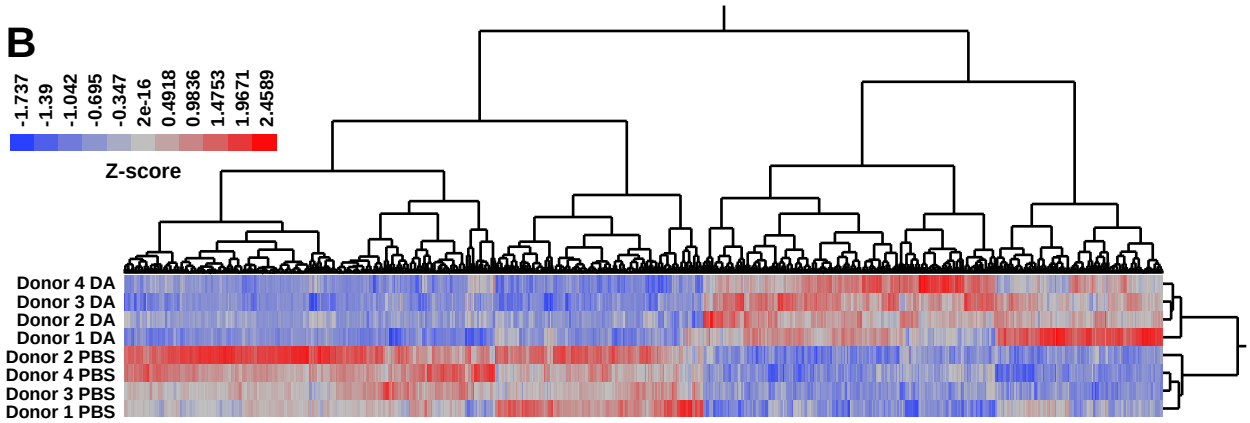
B
-1.737
-1.39
-1.042
-0.695
-0.347
2e-16
0.4918
0.9836
1.4753
1.9671
2.4589
Z-score
Donor 4 DA
Donor 3 DA
Donor 2 DA
Donor 1 DA
Donor 2 PBS
Donor 4 PBS
Donor 3 PBS
Donor 1 PBS

Figure 3

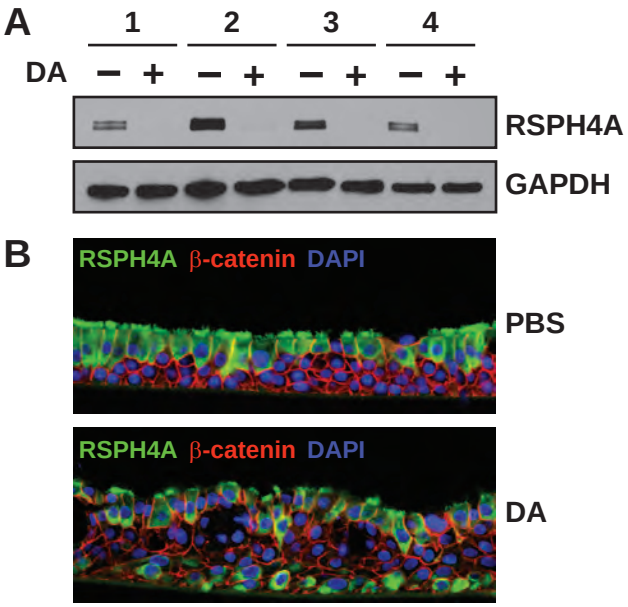
A
1
2
3
4
DA
− + − + − + − +
RSPH4A
GAPDH
B
RSPH4A β-catenin DAPI
PBS
RSPH4A β-catenin DAPI
DA

Figure 4

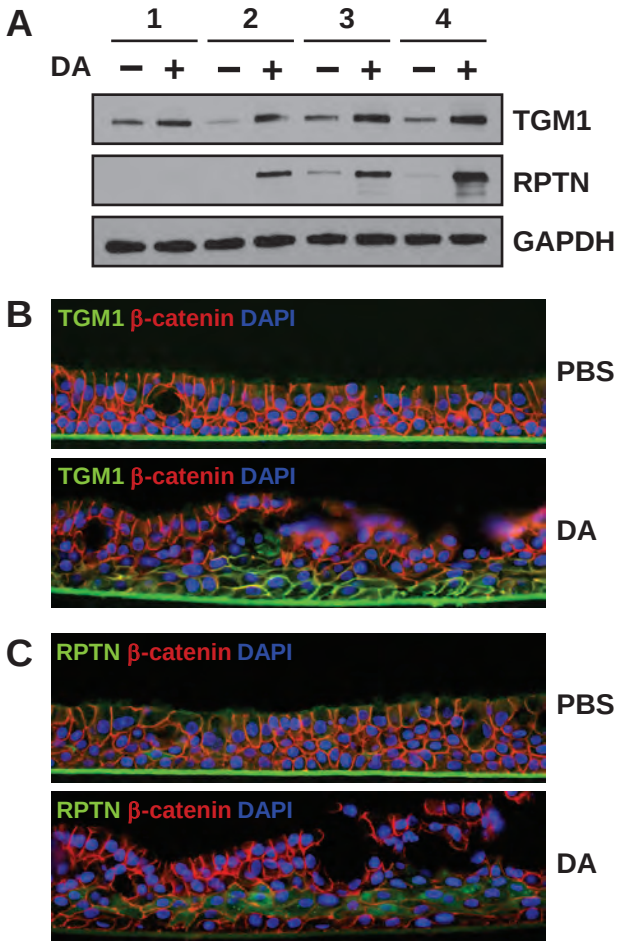
A
1
2
3
4
DA
− + − + − + − +
TGM1
RPTN
GAPDH
B
TGM1 β-catenin DAPI
PBS
TGM1 β-catenin DAPI
DA
C
RPTN β-catenin DAPI
PBS
RPTN β-catenin DAPI
DA

Figure 5

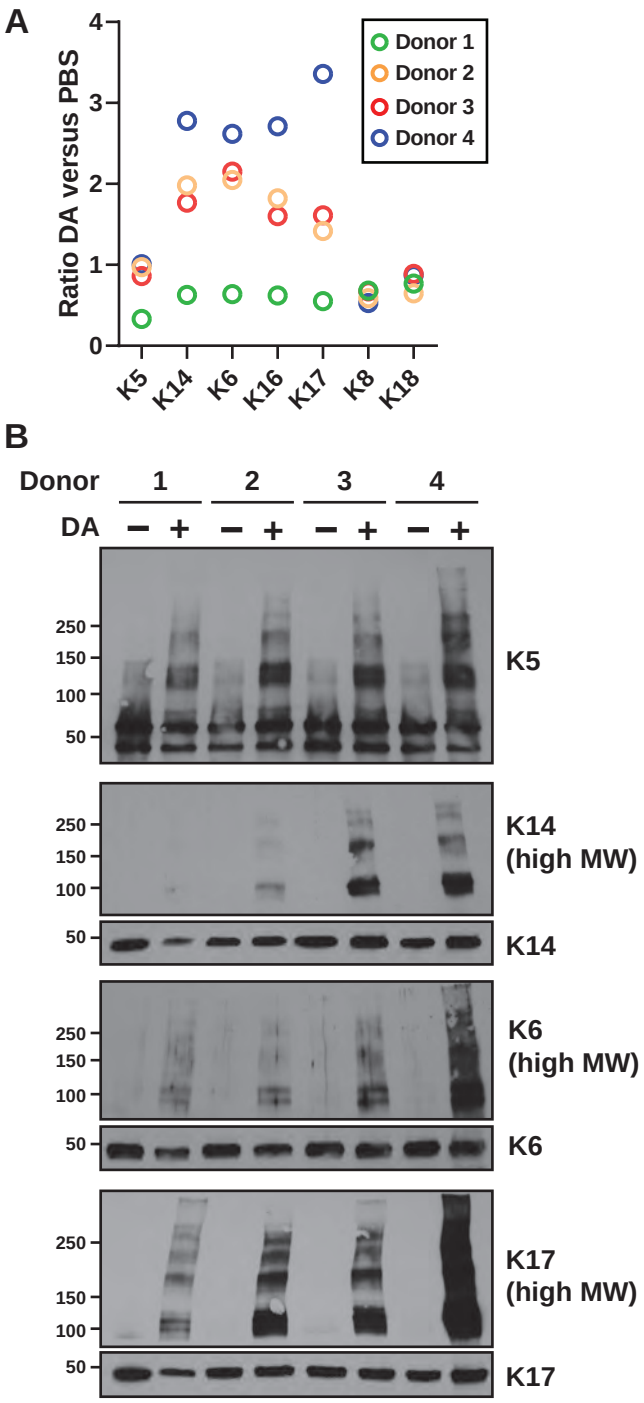
A
Ratio DA versus PBS
0
1
2
3
4
K5
K14
K6
K16
K17
K8
K18
Donor 1
Donor 2
Donor 3
Donor 4
B
Donor
1
2
3
4
DA
− + − + − + − +
250
150
100
50
K5
K14
(high MW)
K14
K6
(high MW)
K6
K17
(high MW)
K17

Figure 6

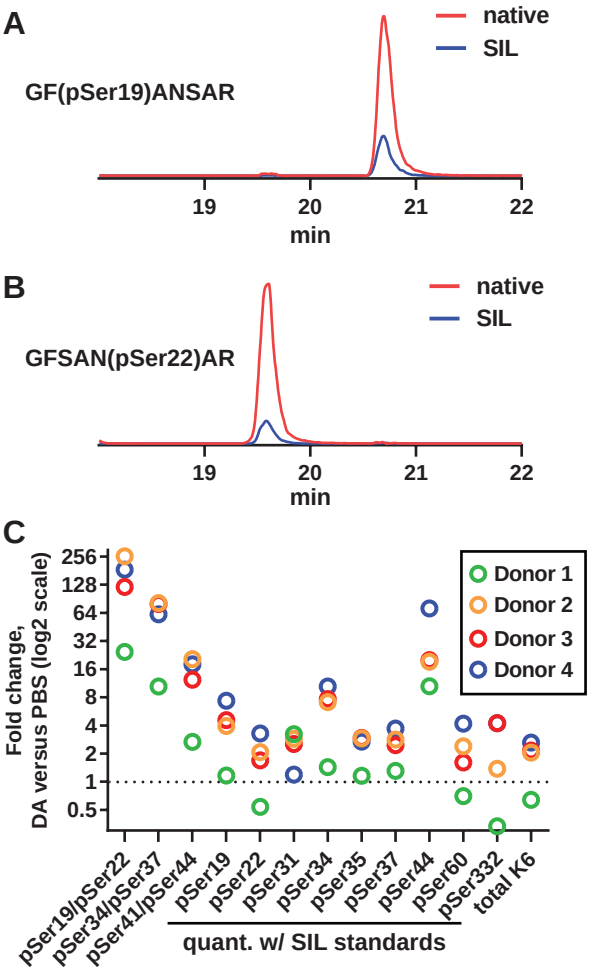
A
native
SIL
GF(pSer19)ANSAR
19
20
21
22
min
B
native
SIL
GFSAN(pSer22)AR
19
20
21
22
min
C
Fold change, DA versus PBS (log2 scale)
256
128
64
32
16
8
4
2
1
0.5
Donor 1
Donor 2
Donor 3
Donor 4
pSer19/pSer22
pSer34/pSer37
pSer41/pSer44
pSer19
pSer22
pSer31
pSer34
pSer35
pSer37
pSer44
pSer60
pSer332
total K6
quant. w/ SIL standards